The Thesis Committee for Rangga Yadi Putra
Certifies that this is the approved version of the following thesis:

Integrated System of Solar Simulator, Photovoltaic Panel, and Single Sensor Load Voltage Maximum Power Point Tracking (MPPT)

APPROVED BY
SUPERVISING COMMITTEE:

Surya Santoso, Supervisor

Ross Baldick

Integrated System of Solar Simulator, Photovoltaic Panel, and Single Sensor Load Voltage Maximum Power Point Tracking (MPPT)

by

Rangga Yadi Putra, B.S.

Thesis

Presented to the Faculty of the Graduate School of

The University of Texas at Austin

in Partial Fulfillment

of the Requirements

for the Degree of

MASTER OF SCIENCE IN ENGINEERING

The University of Texas at Austin

May 2017

Dedication

This works is dedicated to my parents, sisters, and brother.

Acknowledgements

I would like to express my sincere gratitude to Dr. Santoso as my supervisor, for the opportunity to work in the ASPIRE lab and for his valuable guidance and support of my research. I would also like to thank Dr. Baldick for reading this thesis.

I gratefully acknowledge Tuan Ngo, Quan Huy Nguyen, Min Lwin, Hunter B Estes, and Harsha P. for insightful discussion and advice while I was completing this work. I would also like to thank the member of ASPIRE for their assistance in the lab.

Abstract

Integrated System of Solar Simulator, Photovoltaic Panel, and Single Sensor Load Voltage Maximum Power Point Tracking (MPPT) Algorithm

Rangga Yadi Putra, M.S.E.

The University of Texas at Austin, 2017

Supervisor: Surya Santoso

The work reported herein describes the design, analysis, and construction of a 50-W integrated photovoltaic (PV) solar simulator apparatus. It consists of 100-W PV panel, dc-dc converter, maximum power-point tracker, and an artificial light source from four 400-W metal halide light bulbs. The primary function of the apparatus is to simulate a wide range of solar irradiance profiles. Its accuracy is determined by the relative similarity to a given solar irradiance profile. This work begins by reviewing state of the art solar simulators. It covers the type of solar simulators, sources of artificial light, and the configuration and components of simulator. The review is the starting point for conceiving a preliminary simulator design. A computer simulation using Matlab/Simulink is then used to refine the integrated system. Based on this simulation, the complete integrated system is constructed and then validated. Component-level validations are performed by evaluating inputs and outputs of each component. The system-level validations are done by

simulating actual solar irradiance profiles obtained from field measurements and comparing the PV power output profiles to the corresponding irradiance profiles.

Table of Contents

List of Tables

List of Figures

Chapter 1: Introduction

1.1 MOTIVATION

For years, most people have depended on conventional and non-renewable energy such as natural gas or oil as their primary energy source. However, the process of extracting this energy is invasive and destroys the environment around the mining areas. In addition, converting fossil fuel into other energy by burning, produces harmful byproducts that are released into the environment. The increase of carbon dioxide gasses in the air and water pollution are the most common effects of fossil fuel use. On the other hand, there are Renewable energy sources, which are defined as resources that will be naturally replenished and which include sunlight, wind, rain, tides, waves, and geothermal. Renewable energy offers significant possibility of a cleaner and safer environment, and also shall contribute to world's energy security.

Among these renewable energies, solar photovoltaic (PV) is one of the fastest growing energy sources, with an annual growth rate of 60% over the last 10 years [1]. At the beginning of its utilization, the primary market for PV was an off-grid application. However, now over 78% of the global market is grid connected application. As the utilization of grid-connected PV continues to grow, the potential impact on grid's stability and operation also grows. Therefore, the intensity of study and research of PV systems behavior shall increase to solve the issues, and thus increase the PV utilization even further and meet energy demand.

Power generated by PV depends on the irradiance received by the panel at a particular time. As the actual solar irradiance fluctuates according to weather conditions and is not easy to be predicted, thus the behavior PV systems are hard to be observed. Hence, a controllable indoor test facility using artificial light under certain conditions will aid the observation of the behavior or impact of PV systems. The final purpose of this experiment is building a solar simulator which is able to simulate actual solar irradiance profile and generate the maximum possible power from PV panel.

There are several important components in building a complete solar simulator. The first one is controllable artificial light and a photovoltaic (PV) panel. In the first sequence of the simulator, the artificial light generate illumination according to actual solar irradiance profile which will be absorbed by PV panel. Any failure or misbehavior of these components will propagate to the rest of the system. Thus, it is important to ensure that the artificial light matching the sun spectrum and all of the generated light hits the panel with acceptable light losses so that the output power of the panel is maximized and predictable.

The second component is DC-DC converters which has an impedance matching capability. To obtain maximum power transfer from a source which in this case a PV panel that has a finite internal resistance, the resistance of the load must be equal to the resistance of the source as viewed from its output terminal. And therefore, to ensure that the PV panel generates and transfers its maximum possible power, a DC-DC converter is required. The third component is a Maximum Power Point Tracker (MPPT) algorithm, which control the DC-DC converter and operate the PV panel in maximum operating point. The algorithm will be embedded into a microcontroller that has an analog to digital converter (ADC) and

a digital to digital converter (DAC) capability which is required to link the algorithm and the analog DC-DC converter circuit.

The experiments will occur in several steps. First, several types of artificial light, DC-DC converters, and MPPT algorithms will be described and discussed. Thus, one from each of these components will be used to construct the complete solar simulator circuit. Second, the complete simulator will be verified by computer simulation using Matlab/Simulink. Third, based on the first and second steps, the actual circuit will be built and validated. The validation of each of the components will be done by observing input and output. As for the complete solar simulator, it will be validated by simulating the actual solar irradiance profile and observing the simulation result. Finally, the analysis of the simulator result will be described and discussed.

1.2 THESIS OUTLINE

This thesis consists of five chapters and is organized as follows:

Chapter 1 introduces the objective of this works which is involves developing a solar simulator and describing its main components. It also defines and compares conventional energy and renewable energy. Furthermore, it describes briefly the advantages of renewable energy, in particular, solar energy as a potential alternative energy source. This chapter also provides a brief summary of the content and the organization of this thesis.

Chapter 2 focuses on generation of artificial and the control of its luminosity using a microcontroller. The chapter begins by reviewing the existing standard of artificial light

for solar simulator purposes and then compares several types of light sources in greater detail. The character of the PV panel that is used in this study will be described. This chapter also provides the actual solar irradiance data and conversion to an analog signal so that its profile could be simulated and controlled. The configuration of artificial light, control, and signal conditioning will be presented and discussed in detail.

Chapter 3 primarily describes DC-DC converters and Maximum Power Point Tracker (MPPT) which control the converter. This chapter will briefly describe the I-V curve characteristic of PV panel and what it mean to maximize its power. This experiment will compare several types of DC-DC converters and Boost converter that will be implemented in this experiment will be discussed in detail. A current study about MPPT algorithm will also be reviewed, several types of MPPT will be compared, and Single sensor load voltage based MPPT as the proposed algorithm for this study will be described in detail. Final configuration and components of complete MPPT which includes the DC-DC converters, MPPT algorithm, and Voltage sensor will be presented in detail. In addition, this chapter will provide the simulation result of Single sensor load voltage based MPPT.

Chapter 4 presents the validation of the solar simulator circuit. First, the input and output of each component will be verified. Second, the solar simulator will be validated by simulating the actual solar irradiance profile. Thus, the output of the simulator will be observed and discussed. The performance of the simulator with and without MPPT algorithm will be presented. Finally, the analysis of simulation scenario and simulator's performance including its time response in reaching MPP will be discussed.

To conclude this thesis, Chapter 5, summarizes major points, and considers the future potential for research.

Chapter 2: Solar Simulator

2.1 INTRODUCTION

In this chapter, the terms solar simulator refers to artificial light, PV panel, and illumination control. ASTM E927-10 states that a solar simulator is a device that works as an artificial sun and provides its natural light approximately [2]. The purpose is to provide a controllable indoor test facility which is unaffected by the weather outside. In this experiment, the solar simulator will be used to simulate actual solar irradiance profile at particular places and thus to observe the output power of the PV panel. The irradiance profile shall represent the condition during a bright sunny day, cloudy day, or when a cloud passes over and covers the PV panel.

2.2 SOLAR SIMULATOR CLASSIFICATION

IEC 60904-9 and ASTM E927-10 are the commonly used standard for the solar simulator in performance testing of a PV panel. According to those standards, there are three variables which determine the classification of an artificial light: Spectral Content, Spatial Uniformity, and Temporal Stability [2][3]. Table 2.1 summarizes the classification of a solar simulator based on ASTM E927-10.

1. Spectral content

   Sunlight covers all electromagnetic spectrum of light from infrared to near-ultraviolet wavelength therefore it is used as standard of full spectral light. Figure 2.1 shows the spectral content of sunlight. The closer the spectral content of an

artificial light is to the sun, the better of solar simulator is at simulating the actual condition.

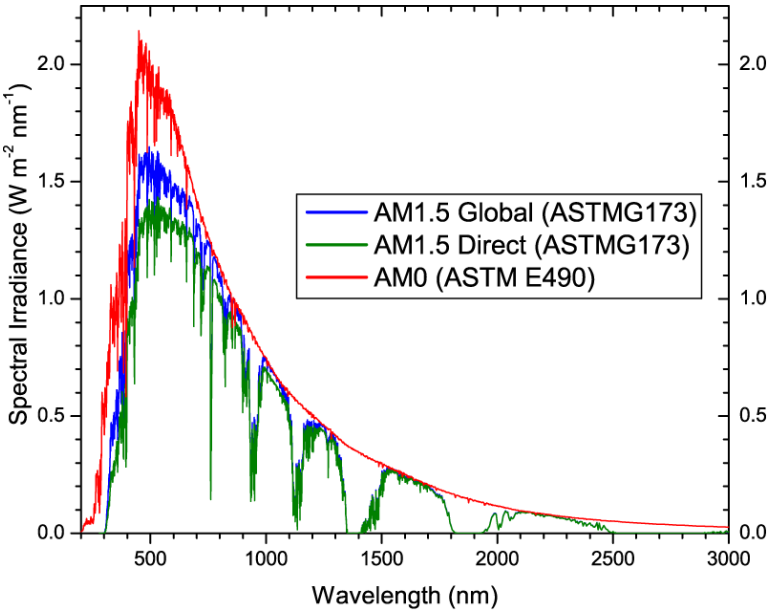

Figure 2.1. Sunlight's Spectral Contents

2. Spatial uniformity

During a sunny day without any obstacle from the cloud, the irradiance of sunlight measured at several points at a certain location is uniform. Thus, the irradiance of sunlight is uniform. In fact, it is considered to be the most uniform light source. The more uniform the artificial light is when illuminating specific plane such as PV panel, the closer is the performance of the simulator to the actual condition.

3. Temporal stability

This variable is defined as the stability of the light beam over a period of time. Sun's irradiance is very stable over time. Again, the more stable the artificial light irradiance is over a period of time, the better the solar simulator performs.

Classification	Spectral Match	Irradiance Spatial Non-Uniformity	Temporal Instability
Class A	0.75-1.25	2%	2%
Class B	0.6-1.4	5%	5%
Class C	0.4-2.0	10%	10%

Table 2.1. Table: Solar Simulator Classification (ASTM E927-10)

2.3 TYPE OF SOLAR SIMULATORS

Based on the time or frequency of the usage, a solar simulator can be divided into three categories:

1. Continuous

This is the type of artificial light source which consists of continuous illumination, and it is usually used of low intensity testing, from less than 1 sun up to several suns. 1 sun is defined as the nominal full sunlight intensity on a bright clear day, which measures 1000 W/m^2. For simulator purpose, this experiment will focus on building a continuous type solar simulator.

2. Flashed

Flashed type simulator is similar to the flash light that is used in photography and it uses flash tubes with a typical duration of several milliseconds

and at a very high intensity of up to several thousand suns. This simulator is often used to prevent heat build-up on the device under testing conditions.

3. Pulsed

Pulsed type simulator uses a shutter to quickly block or unblock the light from a continuous source. Basically, this type is a compromise between continuous and flashed simulator, having the disadvantage of high power usage and relatively low intensity of continuous type and advantage of stable output intensity, spectrum, and low thermal loads of flashed type.

2.4 TYPES OF ARTIFICIAL LIGHT

2.4.1 Xenon Arc Lamps

These lamps are the most widely used in solar simulator because the output light of the lamp is similar to sunlight spectrum outside the atmosphere (AM0). There are, however, large infra-red "spikes" within its spectral content as shown in Figure 2.2. Even so, solar simulator using IR filtered xenon arc source will provide a crude match to AM0/AM1.5. Xenon arc lamps are expensive compared to other arc sources because of increasing demand and limited global supply of xenon.

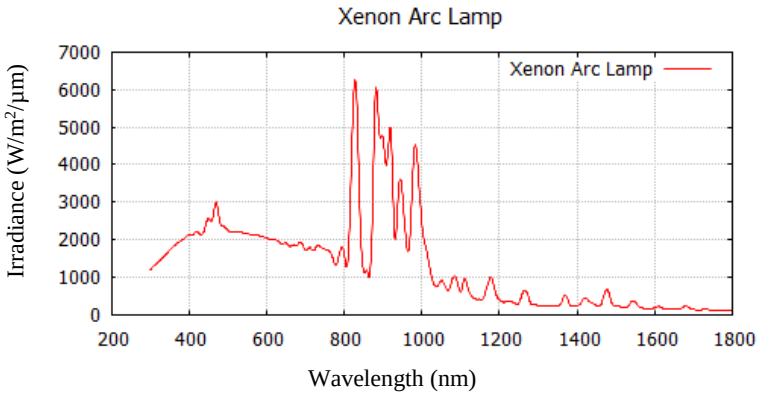

Figure 2.2. Xenon Arc Spectral Content [4]

2.4.2 Metal Halide Arc Lamps

As an alternative to Xenon Arc, Metal Halide Arc lamps are cheaper with greater temporal stability. The infrared spectral is much lower compared to xenon. Moreover, an unfiltered metal halide arc lamp has already produced a B class spectral match. Figure 2.3 represents the spectral content of Metal Halide Arc Lamps.

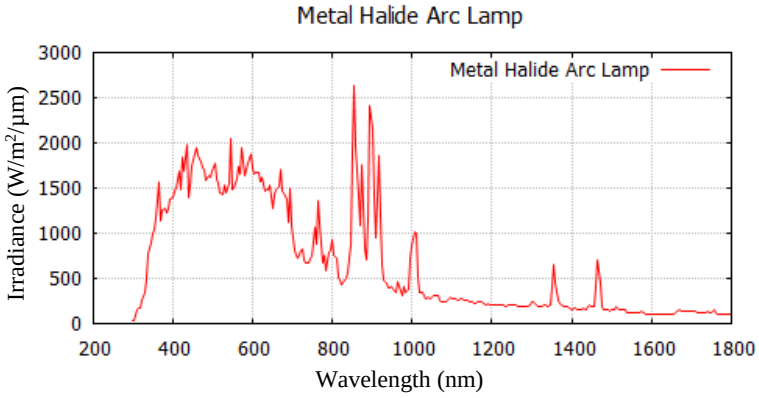

Figure 2.3. Metal Halide Arc Lamp Spectral Content [4]

2.4.3 Light Emitting Diode (LED)

LED lamps have much lower energy consumption and longer lifetime compared to arc lamps. They are, however, only available in discrete wavelengths. Each type of LED produces a specific spectral content and has a relatively narrow band of wavelength. Simulating sunlight which has full spectral content required a combination of several different types of LED. Moreover, commonly available LED does not cover the full spectrum required to construct the spectral content of sun.

2.4.4 Quartz Tungsten Halogen (QTH) Lamps

QTH lamps provide an excellent match in the infra-red region but a very poor match across visible range. The lamps are commonly used for specific purpose solar simulator such as multi-junction solar cells for space applications. Figure 2.4 shows the spectral content of the lamp.

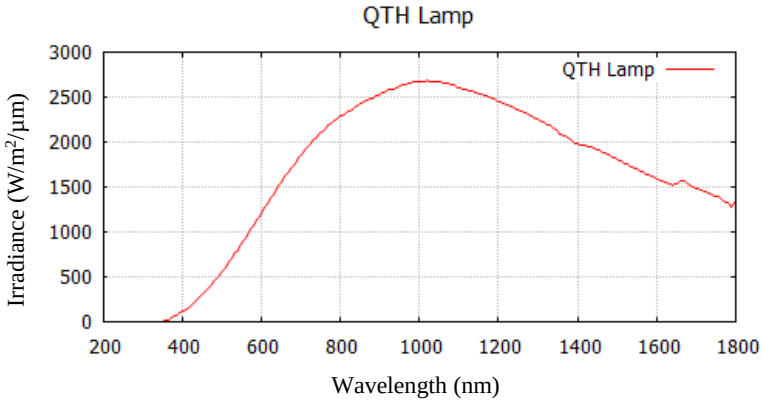

Figure 2.4. QTH Spectral Content [4]

2.5 SOLAR SIMULATOR CONFIGURATIONS AND COMPONENTS

Based on the descriptions above, a Metal Halide Arc lamps is selected as an artificial light source because of its lower cost, stability, and relatively good spectral content match (class B).

Generally, the luminous efficacy of metal halide is 65-90 lumens/Watt. Lumens is defined as the total quantity of visible light emitted by a source. Then based on [26], the illumination of sun measured during a bright day is 100,000 lux. Where Lux is the amount of light on a given area. For example, a light bulb with 1000 lumens and spread its light into 10 m^2 area, produces a 100 lux of illumination on that area. Thus, in order to get the required power rating of the light bulb, the total area of pv panel and the reflector encapsulated the bulb must be calculated or measured. Figure 2.5 is the visualization of pv panel and reflector. Based on figure 2.5 the total area of pv panel and reflector is 3679.70 in^2 or 2.37 m^2.

Therefore, the required lumens to achieve 100,000 lux is 2.37 m^2 x 100,000 = 237,000 lumens. Assuming the average luminous efficacy of a metal halide is 75 lumens/Watt, then the power required to produce 237,000 lumens is 237,000/75 = 3160 Watt. The maximum rating of continuous adjustable ballast available on market is 400 Watt. Therefore, the maximum rating of a single light bulb is limited to 400 Watt. This implies that to achieve 3160 Watt, it requires 8 x 400 Watt of light bulbs. However, using configuration as shown on Figure 2.5, the maximum light bulb that can be fitted inside the reflector is four and thus the maximum achievable power and lumens are 1600 Watt and 120,000 lumens, respectively. For this particular the area of 2.37 m^2, 120,000 lumens

correspond to 50,632 lux. Based on [25], luminous efficacy of sunlight is 105 lumens/Watt, then the irradiance when light intensity is 50,632 lux (lumens/m^2) is 50,632/105 = 482.2 Watt/m^2. Therefore, the maximum expected output power from pv panel is (482.2 Watt/m^2/1000 Watt/m^2 * 100 Watt) = 48.2 Watts.

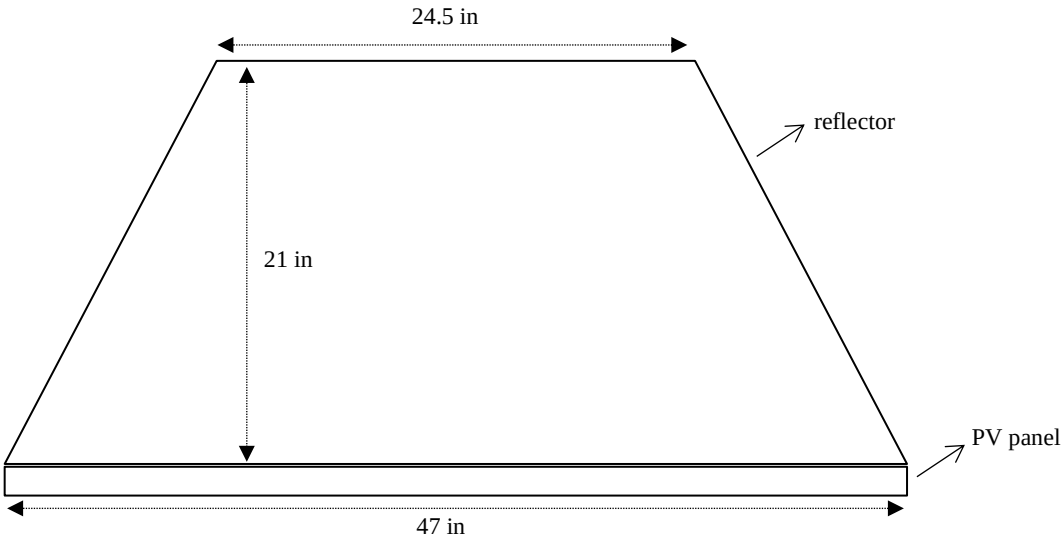

(a)

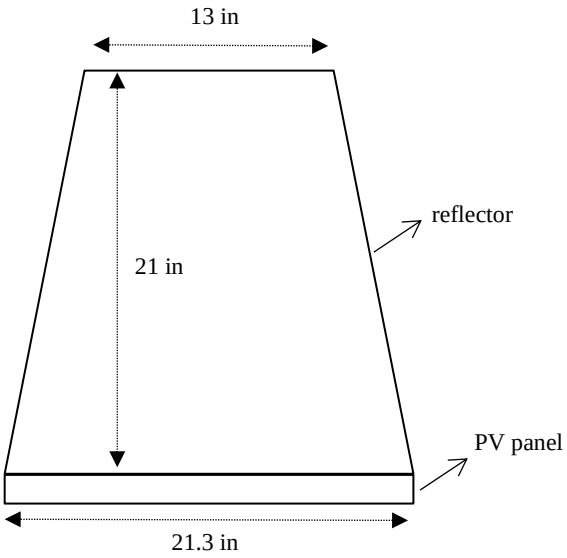

(b)

Figure 2.5. Dimension of PV and Reflector

Metal halide lamps are unique because of their negative dynamic impedance, which makes it necessary to use a ballast as a current limiting element and to provide a stable operating point [5].

Since the purpose of the lamp is to simulate the fluctuation of solar irradiance, the illumination output of the light bulb shall be adjustable. Therefore, this experiments employs a dimmable Metal Halide light bulb with controllable ballast. The ballast will control the amount of power delivered to the light bulbs. Then, the light bulbs produce illumination according to the power they received.

Currently, in the commercial market, the widest range of an adjustable power delivery of a ballast is 50-100%. Furthermore, the input control to the ballast is an analog 0-10 Vdc which corresponds in delivering 50-100% power rating of the bulb.

Based on IESNA Handbook, Figure 2.6 shows that 50-100% input power of metal halide light bulb corresponds to 10-100% of output lumens [6], which implies that using these ballasts, allows the output illuminations of the simulator to be controlled from 10-100%. And thus, the minimum irradiance level that could be simulated by this simulator is 10% of the max irradiance level of the actual solar irradiance profile that is used in this study. In this case, 10% is equal to 140 W/m^2. Therefore, any irradiance profile below 140 W/m^2 cannot be simulated. Section 2.7 will discuss further about solar irradiance profile.

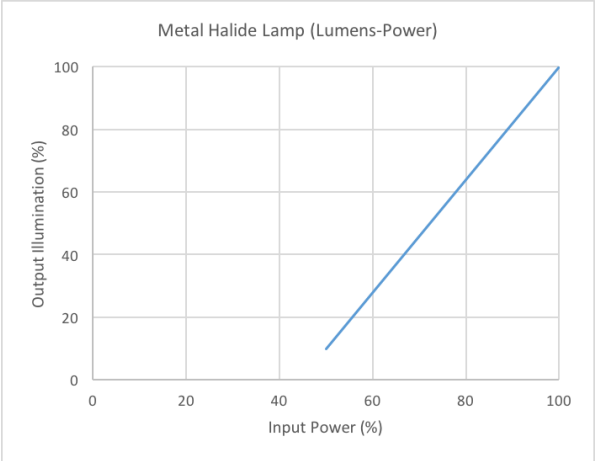

Figure 2.6. Power Input Vs Output Lumens based on IESNA Handbook [6]

There are many ways to generate 0-10 Vdc analog control voltage. For this purpose, Raspberry Pi3 and a digital potentiometer are chosen as the main control for two primary reasons. First, Raspberry Pi uses Python Language which is a high-level programming language that is relatively easy to code. Second, Raspberry Pi3 works just like a typical personal computer. Therefore, it is convenient to store and edit any solar irradiance profile that will be simulated. However, Raspberry Pi 3 does not have an analog output which is necessary to control the ballast. Therefore, a digital potentiometer is used to convert the digital output of Raspberry Pi3 into an analog signal. Figure 2.7 and Table 2.2 shows the overall configuration of the solar simulator and the complete component list, respectively.

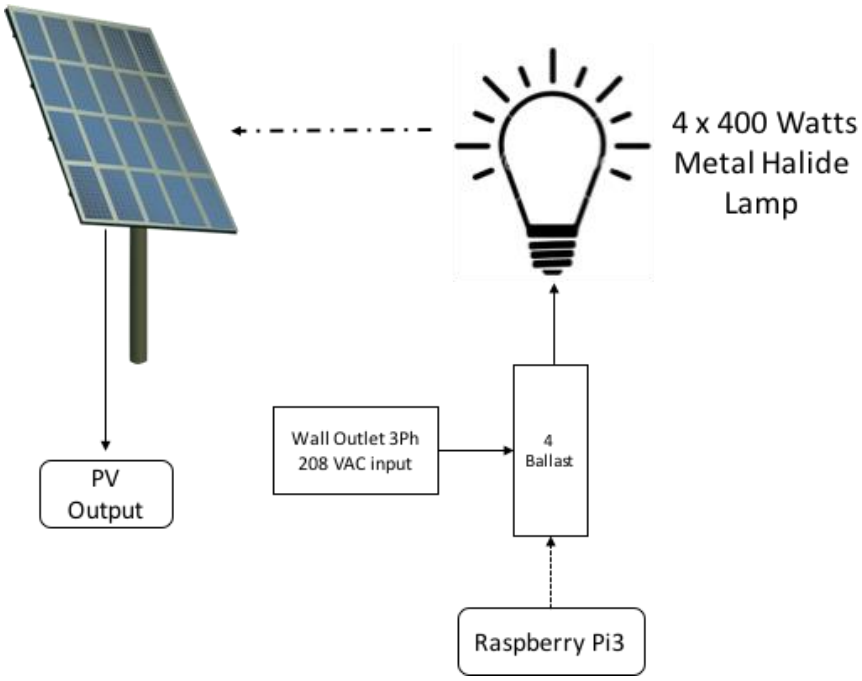

Figure 2.7. Solar Simulator Configuration

No	Item	Specification	Quantity
Main Component			
1	Artificial Light	Metal Halide Arc Lamp 400 Watt	4
2	Ballast	Adjustable Power, 50-100%	4
3	PV Panel	100 Watt	1
Controller			
1	Microcontroller Raspberry Pi3		1
2	Digital Potentiometer MCP4131	5 kΩ	1
3	OpAmps, LM6142	24 V	1
4	Resistor	2.4 kΩ	1
5	Resistor	11.3 kΩ	1
6	Resistor	0.8 kΩ	1
7	Resistor	0.5 kΩ	1
8	Capacitor	0.1 uF	1

Table 2.2. List of solar simulator component

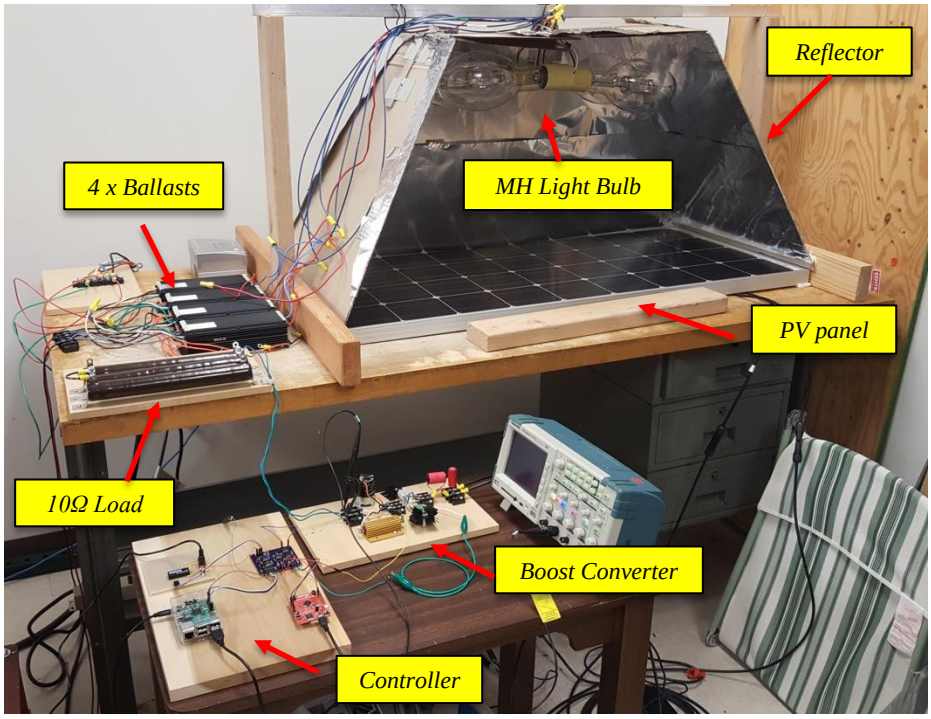

Figure 2.8. Constructed Solar Simulator

2.6 PHOTOVOLTAIC PANEL CHARACTERISTICS

The specification of photovoltaic (PV) panel that is used in this work is listed on table 2.3.

No	Characteristics	Value
1	V_{OC}	22.5 V
2	I_{SC}	5.75 A
3	V_M	18.9 V
4	I_M	5.29 V
5	Dimension	47 x 21.3 x 14 in

Table 2.3. PV Characteristics

The I-V characteristic of PV panel is simulated using a built in pv panel model in Matlab/Simulink. The model is based on the preset PV module from the National Renewable Energy Laboratory (NREL) System Advisor model on January 2014 and user

customized parameters. The PV Array block is using current source, diode, series resistance, and shunt resistance parameters to represent the irradiance and temperature dependent I-V characteristics of the modules [23]. Figure 2.9 shows the block model of the built in pv panel model in Matlab/Simulink.

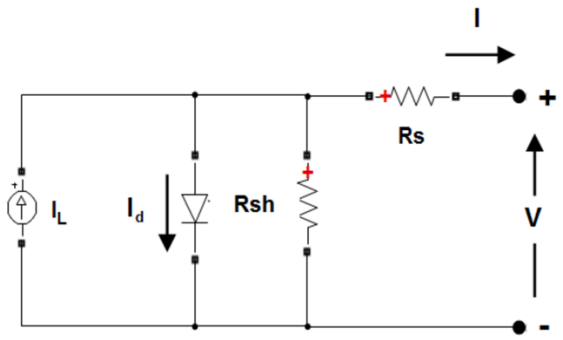

Figure 2.9. Built in PV Panel model in Matlab/Simulink

Inputting the pv characteristics on table 2.3 into the model, the simulation result is shown in Figure 2.10. The maximum power of the pv panel is 100 W. It is achieved when the panel operates at V = 18.9 V and I = 5.29 A.

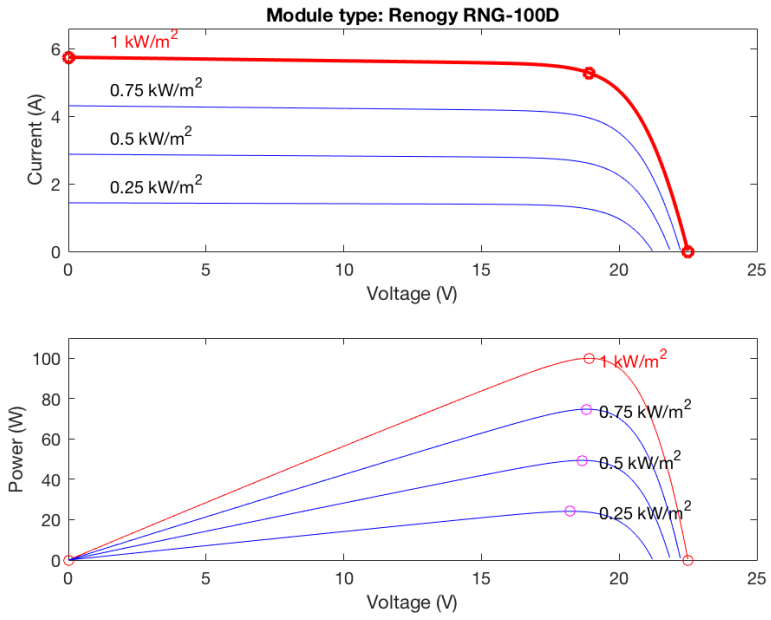

Figure 2.10. I-V curve of PV Panel

2.7 SOLAR IRRADIANCE DATA PROFILE

The solar irradiance data used in this work were collected by the University of Texas Pan-American research team in 2015 [24]. The irradiance data covers a period of 1/1/2015 – 12/31/2015. Measurements were taken from 4 am to 8 pm of the coverage period and the resolution of the measured data is 1 minute.

The captured irradiance data is Global Horizontal, Direct Normal, and Diffuse Horizontal and is measured in units of W/m^2. Direct Normal refers to the transmission of sunlight through the atmosphere without interference. In the case of diffuse horizontal, light is diffused by refraction and aerosols in the atmosphere and some of it continue to travel to reach the surface of the earth. The diffused light can strike the earth at a range of

different angles depending on how it was diffused. Global Horizontal is the sum of Direct Normal and Diffuse Horizontal [7]

Three days with highly fluctuate sunlight irradiance are chosen for the most comprehensive observation and simulator validation. Figure 2.11, 2.12, and 2.13 represent the Global horizontal at 6/1/2015, 7/1/2015, and 8/1/2015, respectively. Figure 2.11 and 2.13 is interpreted as a sunny day with relatively fast cloud movement in the middle of the day up until sunset, which is indicated by a period of high fluctuations in irradiance. On the other hand, figure 2.12 shows a cloudy day except around 2-2.30 pm when the irradiance level represents a clear sky.

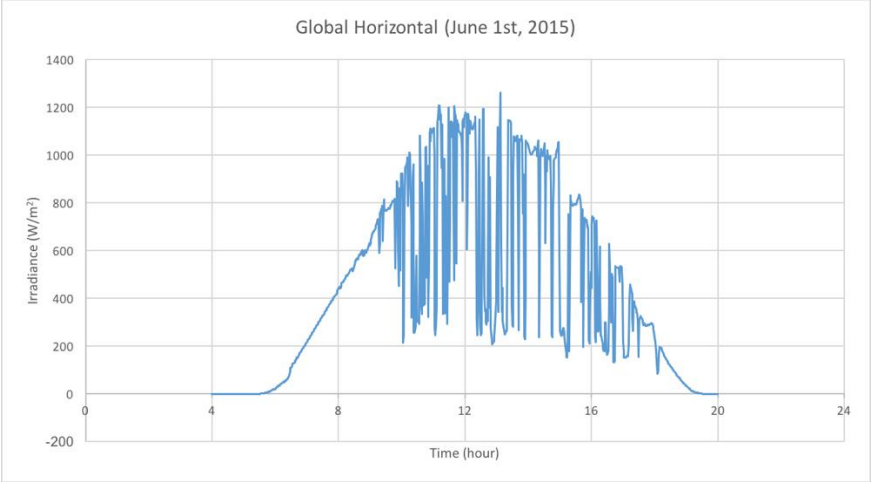

Figure 2.11. Solar Irradiance Profile University of Texas Pan-American Edinburg at 6/1/2015

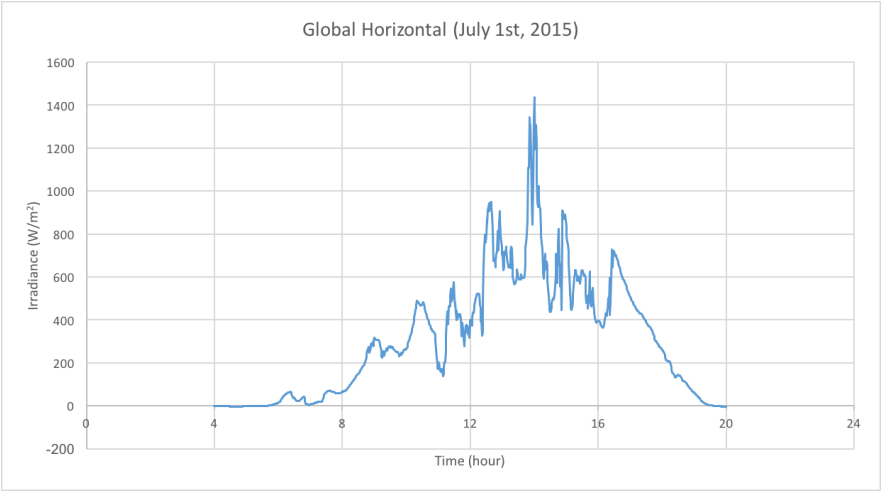

Figure 2.12. Solar Irradiance Profile University of Texas Pan-American Edinburg at 7/1/2015

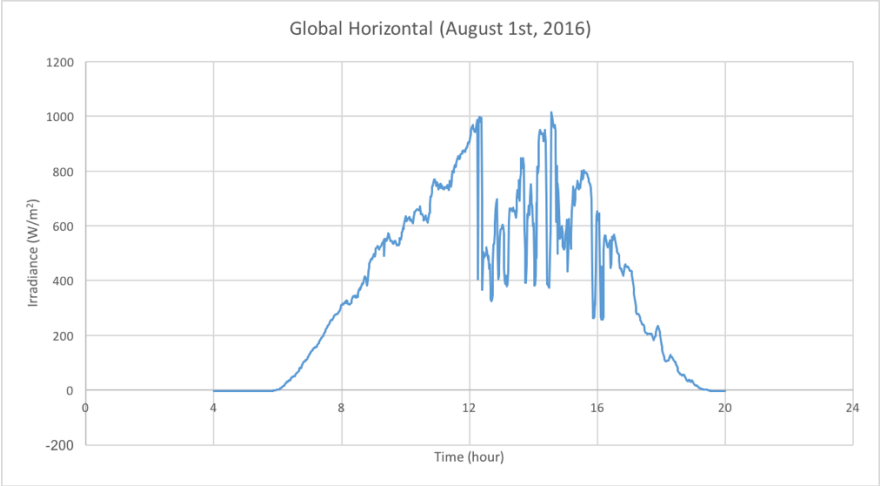

Figure 2.13. Solar Irradiance Profile University of Texas Pan-American Edinburg at 8/1/2015

2.8 DATA CONVERSION

The solar irradiance profile data must be processed through several steps to generate required control signals to the ballast and light bulbs. First, the range of the solar

irradiance data profile is divided into discrete values, in this case, a 7 bit (128 step) digital potentiometer is used as the bridge of digital to analog signal. The range is divided by 128 and therefore the maximum irradiance in the profile, which is 1438 W/m^2 and the minimum irradiance data 0 W/m^2 will correspond to 128 and 0, respectively. In other words, 1 step of digital value represents 11.2 W/m^2 of irradiance.

Second, by using serial communication, the 0-128 data will be delivered to the 7 bit 5 kΩ digital potentiometer. Those values will determine the instantaneous resistance of the digital potentiometer, which the pick-up's pins is connected to 10 V through a voltage divider. The wiper's voltage of the potentiometer will vary according to its instantaneous resistance. In this experiment 0 and 128 corresponds to minimum and maximum resistance of the potentiometer respectively. Third, the voltage at wiper is amplified using noninverting OpAmps so the voltage level matches the input requirement of the ballast, which in this case, 0-10 Vdc. Finally, the instantaneous voltage ranging from 0-10 V drives the ballast that delivers power to the light bulbs so that it will illuminate accordingly. Figure 2.14 represents the circuit to control ballast from Raspberry Pi3.

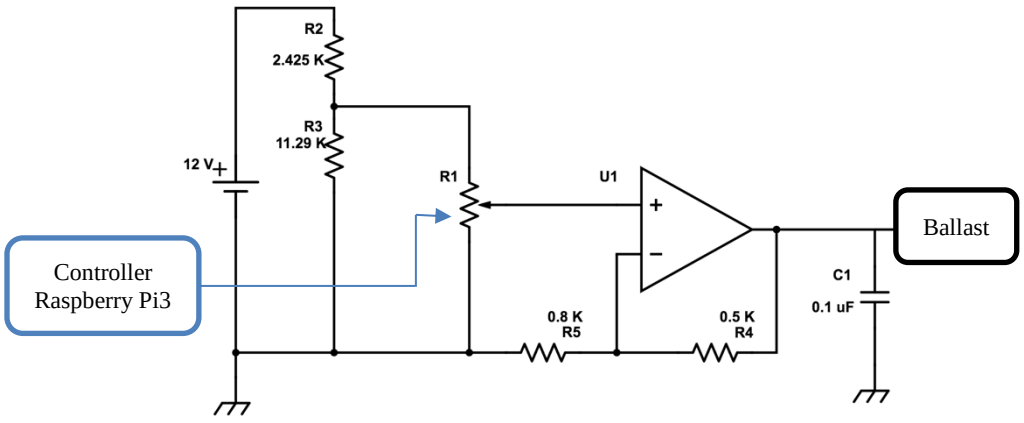

Figure 2.14. Ballast Control Circuit

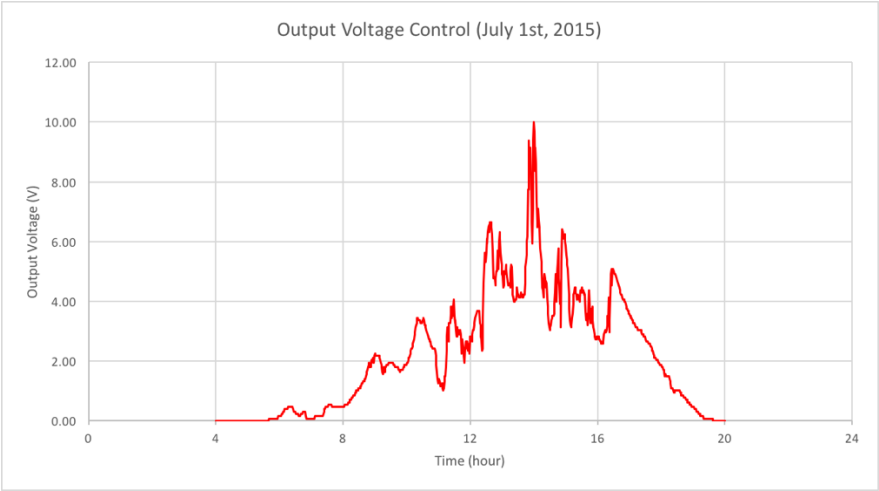

Figure 2.15. Generated Control Voltage for Irradiance Profile 7/1/2015

Figure 2.15 represents the generated control voltage from the irradiance profile on July 1st, 2015. Those control voltages will be sent to ballasts. It can be observed that the curve shape of the generated control voltage follows the irradiance profile. However, because of the use of 7-bit digital potentiometer, the curve shape of the control voltage is not as smooth as the irradiance profile. Using a digital potentiometer of 8-bit or higher will improve the resolution control voltage profile. Nevertheless, for this experiment, a 7-bit digital potentiometer produce enough resolution to follow the actual irradiance profiles.

Chapter 3: DC-DC Converter and Maximum Power Point Tracker (MPPT)

3.1 INTRODUCTION

It is desirable to draw as much as power possible from the PV panel. However, due to impedance mismatch to the load, PV panel, broadly speaking, generates less than half of its maximum power. Therefore, a DC-DC converter that has impedance matching capability is used to maximize the operation of the PV panel. In addition, the MPPT algorithm along with microcontroller will ensure that the panel always operates at MPP in a fluctuating condition of solar irradiance.

The main purpose of this chapter is to describe and compare several types of DC-DC converters and MPPT algorithms, and to choose suitable converter and MPPT algorithm to be implemented in this experiment.

3.2 DC-DC CONVERTER

A DC-DC converter is an electronic circuit that converts a DC source from one voltage level to another level. Converting voltage level in an average sense, DC-DC converters use switches in the circuit that have a particular duty cycle. Figure 3.1 and equation 3.1 represent DC voltage conversion using switches.

So far there are many types of DC-DC converters but, in general, they can be classified into three categories: step-down DC converters, step-up DC converters, and step down/up DC converters. This section will describe one example topology from each

category to show the fundamental DC conversion and impedance matching methods and to compare their advantages and disadvantages.

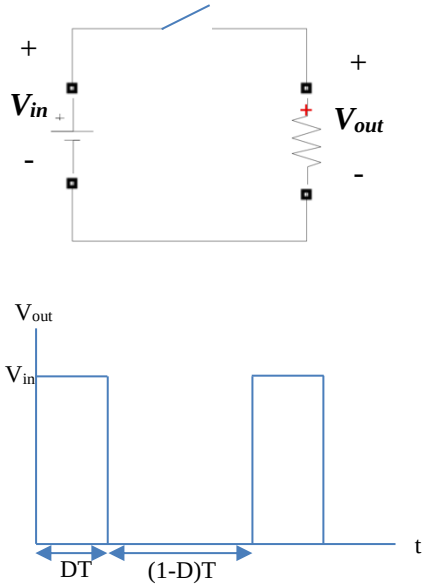

Figure 3.1. DC Conversion using Switch

Based on Figure 3.1, the output average voltage is;

$$V_{out} = DV_{in} \tag{3.1}$$

where D is the duty cycle of the switch.

3.2.1 Step down DC converter

Buck converter is the most popular type of step-down DC-DC converters. Figure 3.2 represents an ideal buck converter.

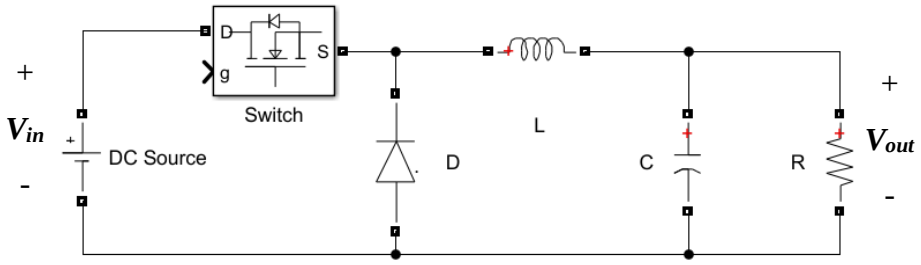

Figure 3.2. Buck Converter Configuration

The DC source is assumed ideal and ripple free. The switch opens/closes at a fixed frequency and the duty cycle is adjusted to control V_{out}. Furthermore, C is assumed to be large so that V_{out} is ripple free. In an average analysis, the relation between V_{out} and V_{in} can be derived with a the following steps;

1. Switch close for DT seconds

   When the switch is closed, we can see the switch is a short circuit. The diode is reversed biased and is thus an open circuit. The ideal buck converter circuit now looks like Figure 3.3.

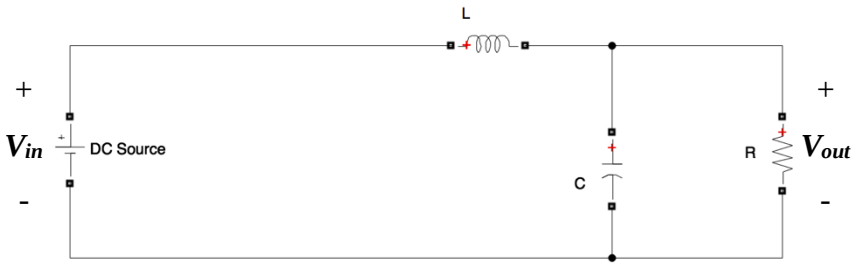

Figure 3.3. Buck Converter Equivalent Circuit, *Switch Closed*

$$v_L = V_{in} - V_{out} \tag{3.2}$$

$$v_L = L\frac{di_L}{dt} \tag{3.3}$$

$$V_{in} - V_{out} = L\frac{di_L}{dt} \tag{3.4}$$

$$\frac{di_L}{dt} = \frac{V_{in} - V_{out}}{L} \tag{3.5}$$

2. Switch open for (1-D)T seconds

   When the switch is open, the inductor current (I_L) continues to flow, and the diode is forward biased (short circuit). The ideal buck converter circuit now looks like Figure 3.4.

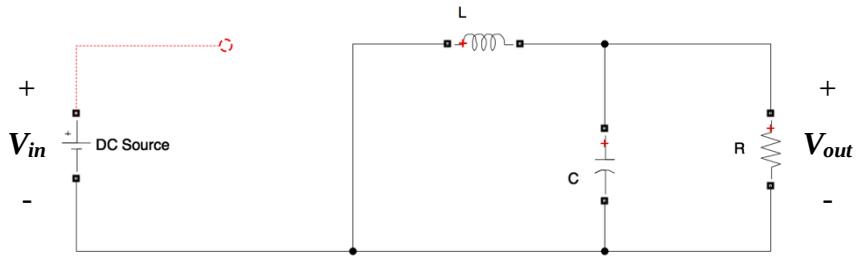

Figure 3.4. Buck Converter Equivalent Circuit, *Switch Open*

$$v_L = -V_{out} \tag{3.6}$$

$$v_L = L\frac{di_L}{dt} \tag{3.7}$$

$$-V_{out} = L\frac{di_L}{dt} \tag{3.8}$$

$$\frac{di_L}{dt} = \frac{-V_{out}}{L} \tag{3.9}$$

3. The average voltage across an inductor (L) is zero and thus,

$$v_{Lavg} = D(V_{in} - V_{out}) + (1 - D)(-V_{out}) = 0 \tag{3.10}$$

$$DV_{in} = DV_{out} + V_{out} - DV_{out} \tag{3.11}$$

$$V_{out} = DV_{in} \tag{3.12}$$

4. The inductor current over a period of time

   As derived from equation 3.5 and 3.8, Figure 3.5 shows the inductor current when the switch is open and closed. The average current, which is the mid-point between I_{max} and I_{min}, is the output current.

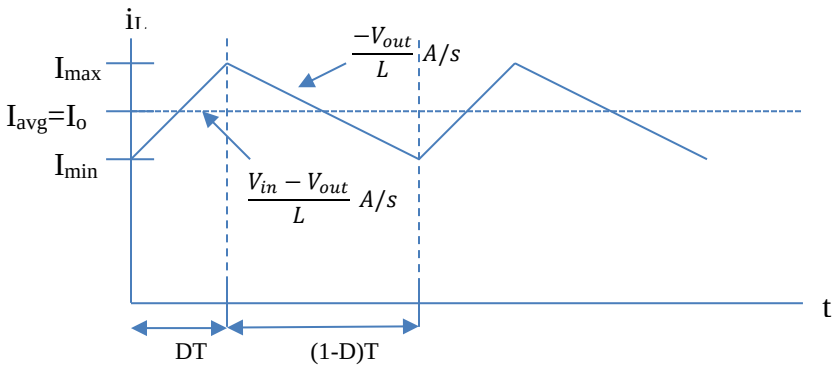

Figure 3.5. Inductor Average Current

5. Impedance matching using Buck Converter

   If we suppose that the converter is connected to a load, then the overall circuit will resemble Figure 3.6, and the impedance that is sensed by input side, R_{equiv}, is represented in Figure 3.7.

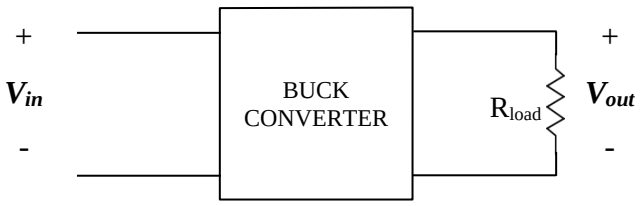

Figure 3.6. Simplified Buck Converter and Load Impedance

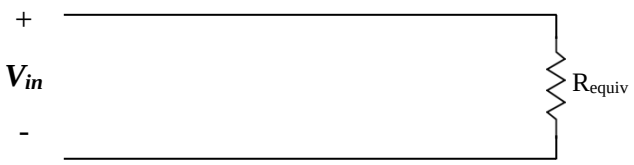

Figure 3.7. Equivalent Impedance seen by Input side

$$V_{out} = DV_{in} \tag{3.13}$$

$$R_{load} = \frac{V_{out}}{I_{out}} \tag{3.14}$$

$$R_{equiv} = \frac{V_{in}}{I_{in}} \tag{3.15}$$

$$\frac{V_{in}}{I_{in}} = \frac{\frac{V_{out}}{D}}{I_{out}D} = \frac{V_{out}}{I_{out}D^2} = \frac{R_{load}}{D^2} \tag{3.16}$$

$$R_{equiv} = \frac{R_{load}}{D^2} \tag{3.17a}$$

The range of D is 0-1, then,

$$R_{equiv} = \begin{cases} \frac{R_{load}}{D^2}; for\ 0 < D \leq 1 \\ \\ \infty\ ;\ \ for\ D = 0 \end{cases} \tag{3.17b}$$

Based on equation 3.17a, the buck converter makes the load resistance larger with respect to the input side since the range of D is 0-1. Thus, when the load resistance is relatively smaller than input or source impedance, a buck converter is suitable to match the impedance and maximize the power transfer.

3.2.2 Step up DC converter

A boost converter is one of the step-up DC converter topologies. Figure 3.8 shows an ideal boost converter.

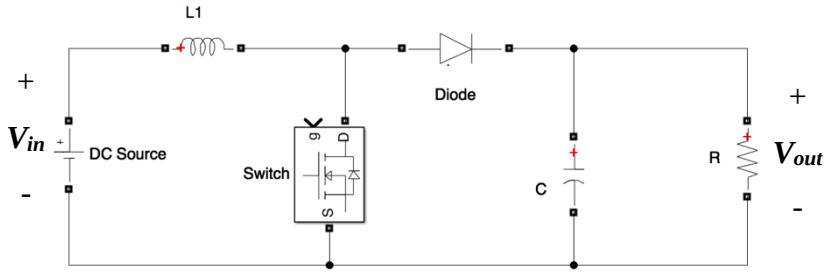

Figure 3.8. Boost Converter Configuration

Using the same approach on analyzing Buck Converter, the DC source is first assumed ideal and ripple free. Then, the switch opens/closes at a fixed frequency and the duty cycle is adjusted to control V_{out}. Furthermore, C is assumed to be large so that V_{out} is ripple free. Finally, in average sense, the analysis of the boost converter is as follows:

1 Switch close for DT seconds

In this condition, the switch is shorted and the diode is reverse biased or open circuit. Figure 3.9 shows the equivalent circuit when the switch is closed.

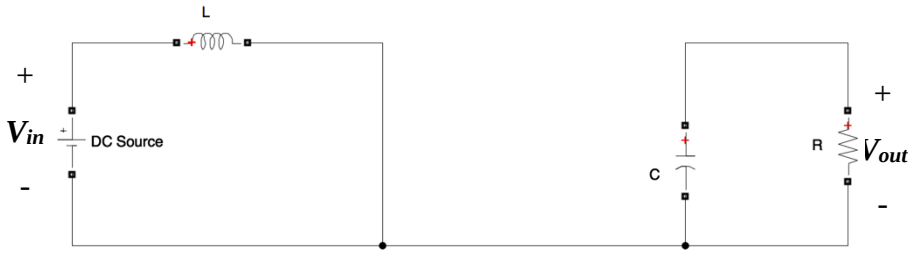

Figure 3.9. Boost Converter Equivalent Circuit, *Switch Closed*

$$v_L = V_{in} \tag{3.18}$$

$$\frac{di_L}{dt} = \frac{V_{in}}{L} \tag{3.19}$$

2 Switch open for (1-D)T seconds

In this condition, the switch is open circuit and the diode is forward biased or short circuited. The equivalent circuit is shown in Figure 3.10.

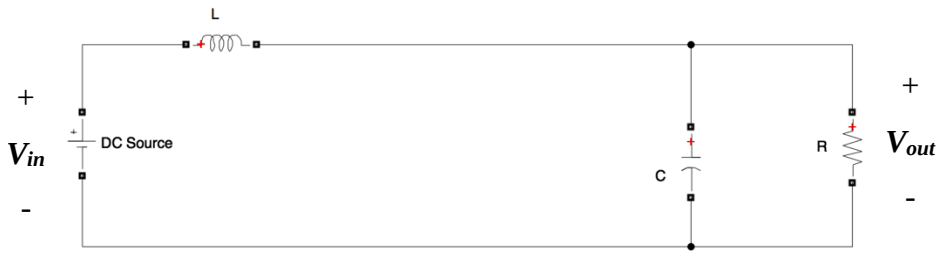

Figure 3.10. Boost Converter Equivalent Circuit, *Switch Open*

$$v_L = V_{in} - V_{out} \tag{3.20}$$

$$\frac{di_L}{dt} = \frac{V_{in} - V_{out}}{L} \tag{3.21}$$

3 The average voltage across an inductor (L) is zero and thus,

$$v_{Lavg} = DV_{in} + (1 - D)(V_{in} - V_{out}) = 0 \tag{3.22}$$

$$V_{out}(1 - D) = V_{in} + DV_{in} - DV_{in} \tag{3.23}$$

$$V_{out} = \frac{V_{in}}{1 - D} \tag{3.24}$$

4 The inductor current over a period of time

As derived from equation 3.19 and 3.21, the inductor's current when the switch is open and close is shown in Figure 3.11. The average current which is the mid-point between I_{max} and I_{min}, is the input current.

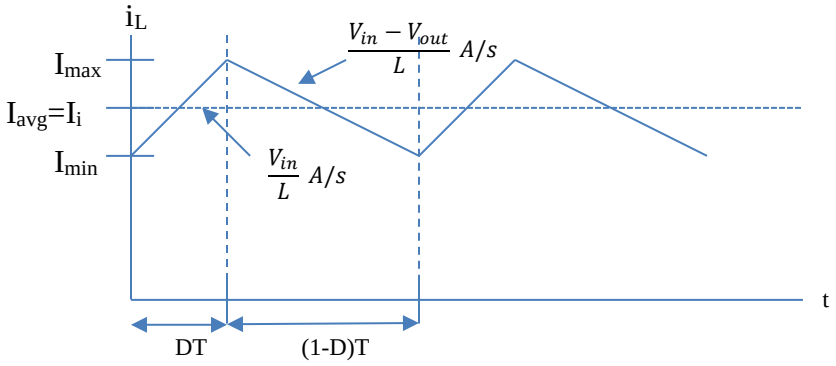

Figure 3.11. Inductor Average Current

5 Impedance matching using Boost Converter

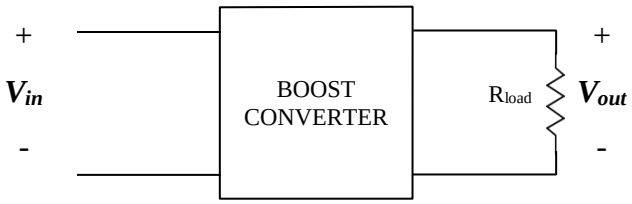

Figure 3.12. Simplified Boost Converter and Load Impedance

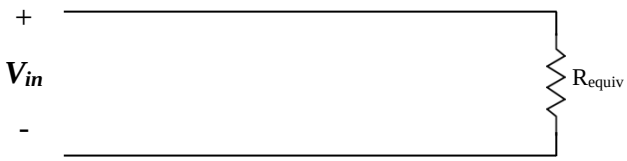

Figure 3.13. Equivalent Impedance seen by Input side

$$V_{out} = \frac{V_{in}}{1-D} \tag{3.25}$$

$$R_{load} = \frac{V_{out}}{I_{out}} \tag{3.26}$$

$$R_{equiv} = \frac{V_{in}}{I_{in}} \tag{3.27}$$

$$\frac{V_{in}}{I_{in}} = \frac{(1-D)V_{out}}{\frac{I_{out}}{1-D}} = \frac{(1-D)^2 V_{out}}{I_{out}} \tag{3.28}$$

$$R_{equiv} = (1 - D)^2 R_{load} \quad (3.29)$$

Based on equation 3.29, the boost converter makes the load impedance smaller with respect to the input side, since the range of D is 0-1. Thus, when the load impedance is larger than input or source impedance, the boost converter can match the impedance and maximize the power transfer.

3.2.3 Step Up/Down DC Converter

SEPIC and buck-boost [8] converters are the most popular topologies for a step up/down DC converter. The difference between those converters is the output polarity. SEPIC has the same polarity as the input while Buck-Boost has a reverse polarity. Depending on the applications, both converters are suitable for adjusting DC voltage up/down. The ideal circuit of SEPIC converter is shown in Figure 3.14.

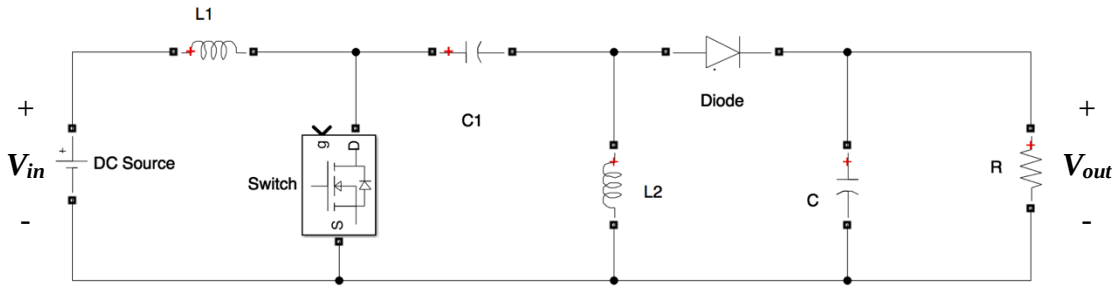

Figure 3.14. SEPIC Converter Configuration

In the ideal SEPIC converter, the values of C1 and C are assumed to be very large so that $V_{C1} = V_{in}$ and V_{out} is ripple free at all the times. Moreover, the DC source is assumed ideal and ripple free. In addition, the switch opens/closes at a fixed frequency. In average sense, the analysis of SEPIC converter is as follows:

1. Switch close for DT seconds

   Using KVL at Switch, C1, L2 Loop, and L2, Diode, C Loop shows that V_{Diode}=-(V_{in}+V_{out}) thus the diode is reverse biased. Figure 3.15 shows the equivalent circuit when the switch is closed. At this condition, Vin charge L1, C1 discharge into L2, and C discharges into load R.

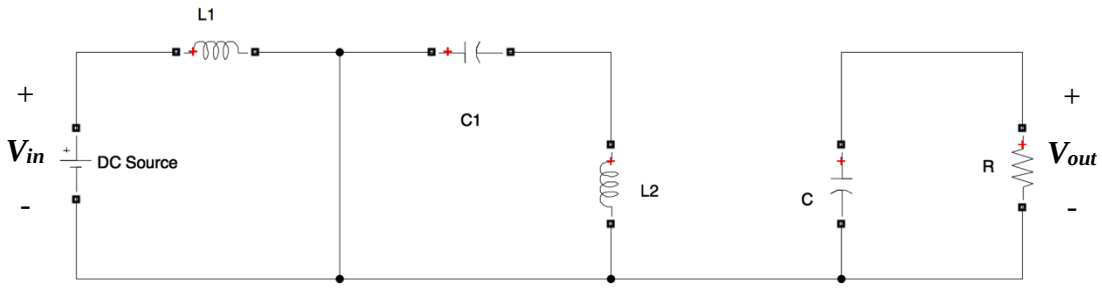

Figure 3.15. SEPIC Converter Equivalent Circuit, *Switch Closed*

$$v_{L1} = V_{in} \tag{3.30}$$

$$\frac{di_{L1}}{dt} = \frac{V_{in}}{L_1} \tag{3.31}$$

2. Switch open for (1-D)T seconds

   Figure 3.16 shows the equivalent circuit when the switch is open. In this case, L1 and L2 are already charged and have to be discharged to C or load. Therefore, the diode is forward biased. In this case L1 discharge through C1 into C and load, L2 discharges into C and load.

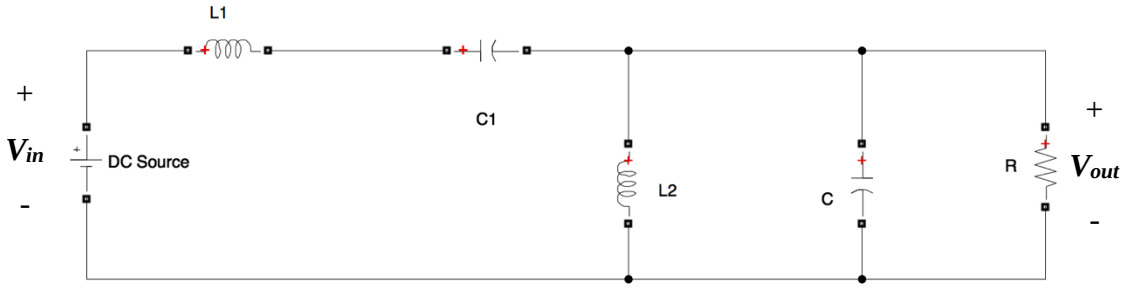

Figure 3.16. SEPIC Converter Equivalent Circuit, *Switch Open*

$$v_{L1} = -(V_{out} + v_D) \tag{3.32}$$

Assume voltage drop across diode is very small;

$$v_{L1} = -V_{out} \tag{3.33}$$

$$\frac{di_{L1}}{dt} = \frac{-V_{out}}{L_1} \tag{3.34}$$

3. The average voltage across an inductor is zero and thus,

$$v_{L1avg} = DV_{in} + (1 - D)(-V_{out}) = 0 \tag{3.35}$$

$$V_{out}(1 - D) = DV_{in} \tag{3.36}$$

$$V_{out} = \frac{DV_{in}}{(1-D)} \tag{3.37}$$

Duty cycle could be varied from 0-1. Based on equation 3.37, therefore, the output voltage of SEPIC converter can be increased or decreased.

4. The inductor current over a period of time

As derived from equation 3.31 and 3.34, the L_1's current when the switch is open and closed is shown in figure 3.17. The average current which is the mid-point between I_{max} and I_{min} is the input current.

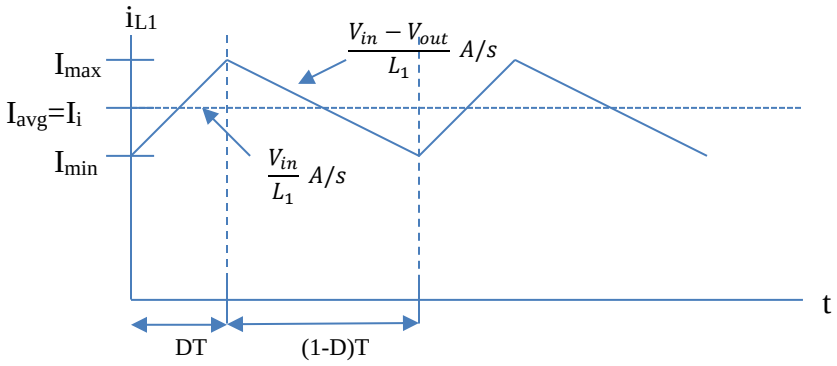

Figure 3.17. L_1 Average Current

5. Impedance matching using SEPIC Converter

Figure 3.18. Simplified SEPIC Converter and Load Impedance

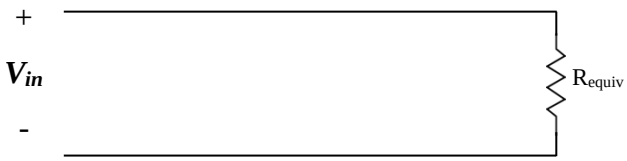

Figure 3.19. Equivalent Impedance seen by Input side

$$V_{out} = \frac{DV_{in}}{(1-D)} \tag{3.38}$$

$$R_{load} = \frac{V_{out}}{I_{out}} \tag{3.39}$$

$$R_{equiv} = \frac{V_{in}}{I_{in}} \tag{3.40}$$

$$\frac{V_{in}}{I_{in}} = \frac{\frac{(1-D)V_{in}}{D}}{\frac{DI_{out}}{(1-D)}} = \frac{(1-D)^2 V_{out}}{D^2 I_{out}} \tag{3.41}$$

$$R_{equiv} = \frac{(1-D)^2}{D^2} R_{load} \quad (3.42)$$

Based on equation 3.42, the SEPIC converter, with a D range of 0-1, is capable of making the load impedance smaller or bigger with respect to the input side. Thus, the SEPIC converter can maximize the power transfer at any output impedance condition.

Table 3.1 shows the summary of V_{out}/V_{in} and R_{equiv}/R_{load} of the converters.

Converter	V_{out}/V_{in}	R_{equiv}/R_{load}
Buck	$\boldsymbol{D}$	$\boldsymbol{\frac{1}{D^2}}$
Boost	$\boldsymbol{\frac{1}{1-D}}$	$\boldsymbol{(1-D)^2}$
SEPIC	$\boldsymbol{\frac{D}{(1-D)}}$	$\boldsymbol{\frac{(1-D)^2}{D^2}}$

Table 3.1. Comparison of Buck, Boost and SEPIC converter

Based on the descriptions above, Boost converter is selected in this study for several reasons. First, Figure 2.7 show the maximum operating point of PV panel which is V_{pv} = 18.9 V and I_{pv} = 5.29 A, thus, the input impedance is R_{in} = 3.57 Ω which is lower than the output resistive load at 10 Ω. Moreover, for simulator purpose, the irradiance will be varied to match the actual irradiance profile, conditions where the irradiance is lower than 1000 W/m^2 occurs many times. This implies that the V_{pv}, I_{pv}, and R_{in} will also decrease, and therefore boost converter is required to increase the input impedance relatively to the output side and reach the MPP. Second, Boost converter offers a simpler topology compared to SEPIC converter which is easier to control, maintain and is also less expensive. In addition, simpler topology means a faster response time of the circuit. Finally, the diode in the Boost converter will make sure that there will be no back current flowing into PV panel. During

conditions where the light is absent, there is possibility of the current flowing from the grid to the panel in Buck Converter topology.

However, special attention must be given to the Boost converter. Based on Figure 3.8, the load must be connected at all times to the output side of Boost Converter, otherwise the output voltage will increase drastically following the voltage rating of the output capacitor which generally is more than 100 V and thus, destroy the circuit. Furthermore, based on equation 3.24, the duty cycle of the gate cannot go anywhere near 1, which theoretically would increase V_{out} into infinity. Therefore, in this experiment, the duty cycle is limited to 0.8.

3.3 MAXIMUM POWER POINT TRACKER (MPPT)

Maximum Power Point Tracker (MPPT) is an algorithm to reach MPP. It is usually used for renewable energy such as PV systems or Wind Turbine. The algorithm usually involves real-time voltage or current measurement from the system. Then the algorithm will suggest an output that changes the voltage or current of the systems operating point. Since it involves algorithm and analog system measurements, an embedded system is suitable to implement MPPT.

Currently, there are many types of MPPT algorithm. However, with respect to DC-DC converters side, they can be classified into two categories; input parameter based and output parameter based. Fractional open circuit voltage [9], fractional short circuit current [10], Hill-climbing [11], Perturb and Observed (P&O) [12], incremental conductance [13], incremental resistance [14], and ripple correlation control (RCC) [15] are among the

popular algorithms that are categorized as input parameter based MPPTs. The input parameter that is involved in the algorithm could be V_{in} or I_{in} or both. Output voltage single sensor [16] and output current single sensor [17] are among the algorithms that are categorized as output parameter based MPPTs. Both type of algorithm can be improved by fuzzy logic, optimization algorithm, or sliding mode control. However, due to the complexity of the algorithm and the need for a digital controller, those methods are not commonly implemented [18]. To compare, input parameter based P&O algorithms and output parameter based Single Load Voltage algorithms will be described and discussed in further detail.

3.3.1 Perturb and Observe (P&O) MPPT

The main idea of P&O technique is adjusting/perturbing the value of some variables and observing the corresponding power change. Voltage, current, or converter's duty cycle could be the perturbed variable. Voltage control is preferable to current control since it is easier to sense and faster to respond when there is a change in solar irradiance. This section will focus on describing P&O algorithm using voltage control. Nevertheless, even though the algorithm use voltage control, it still requires both voltage and current measurement to derive the change in power.

In the basic P&O algorithm, perturbation continues in the same direction whenever the power continuous to increase and reverses the direction whenever the power decreases. Thus, the operating point will move gradually to MPP. However, the operating point will never stop at MPP, and it will oscillate back and forth around the MPP. When the

perturbation step is larger, MPP is reached more quickly and oscillation around MPP is larger. Therefore, the speed of perturbation and size of the step must be selected carefully to reach the MPP fast enough within acceptable oscillation. Figure 3.20 and Figure 3.21 represent the flowchart algorithm and schematic diagram of P&O implementations. The algorithm sequence begins with sensing voltage V(k) and current I(k) of PV panel and calculate the instantaneous power P(k). Then compare the power with the previous iteration P(k-1), and repeat the step until there is a change in power. If the change of power has the same direction as the change of voltage, increase the voltage reference by a perturbation's step of ΔV. On the other hand, if change of power has an opposite direction as change of voltage, decrease voltage reference by ΔV.

P&O technique is extensively used because it has a simple algorithm and is easy to implement. However, some of the research literature mentions that with P&O algorithm, current and voltage operating point of the panel moves away from MPP as solar irradiance levels change rapidly [20]. Moreover, current sensing is more complicated than voltage sensing, especially in a circuit where switching noises are present.

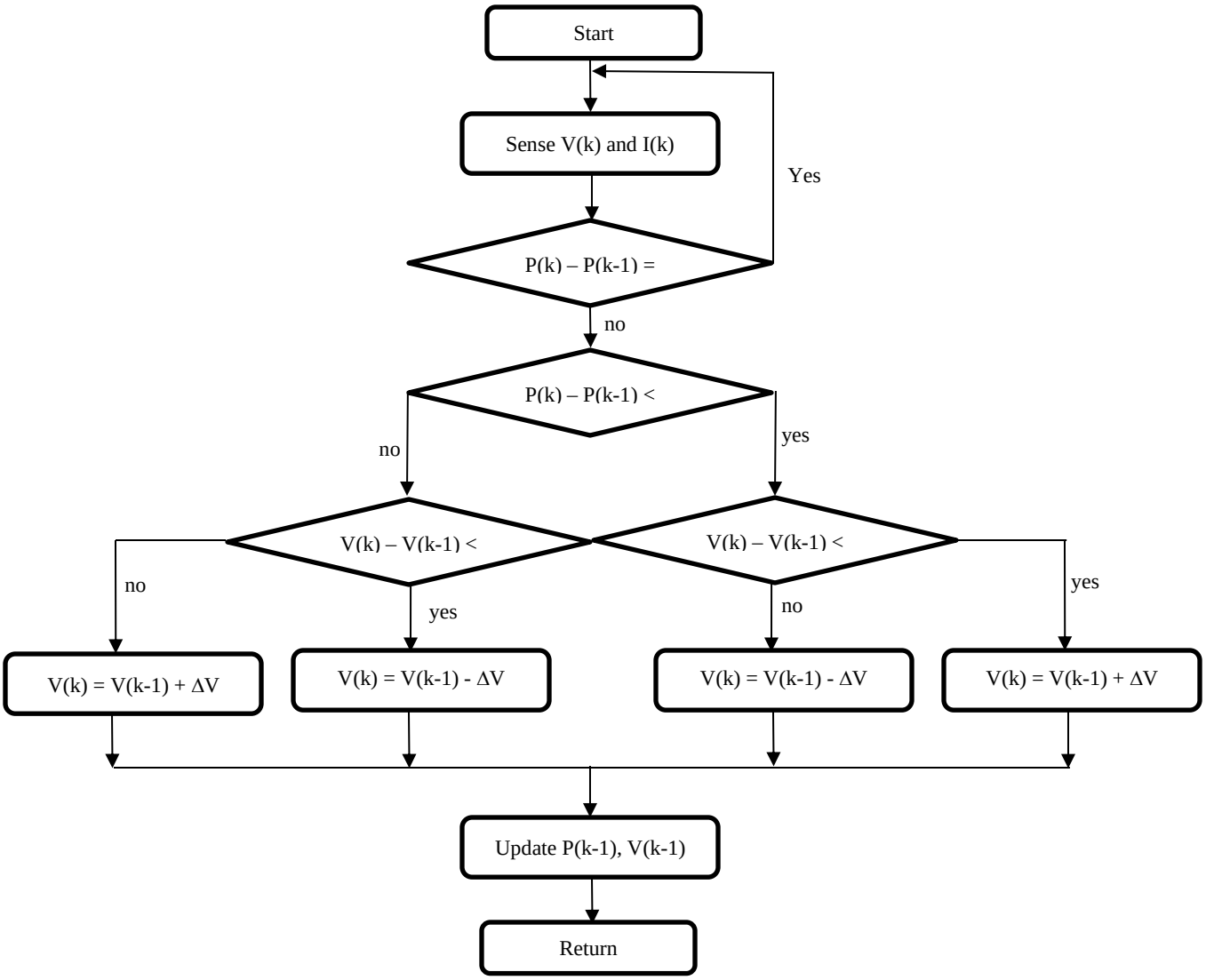

Figure 3.20. Perturb and Observe MPPT Algorithm

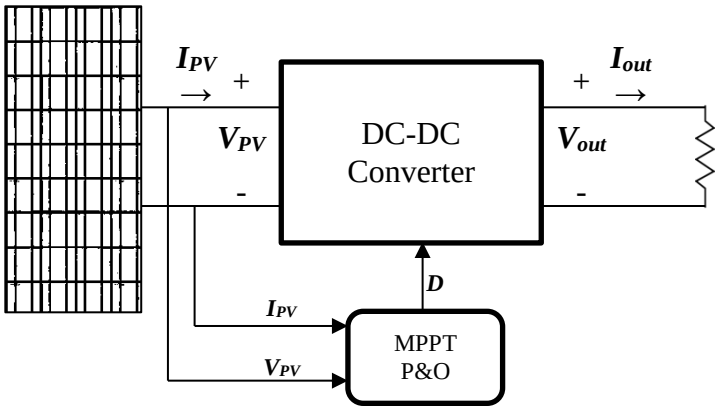

Figure 3.21. Perturb and Observe MPPT Configuration

3.3.2 Single sensor load voltage MPPT

On the output side of a DC-DC converter, voltage and current are linear, which implies that an increase in voltage is followed by an increase in current, and the reverse is also true. It further implies that if either voltage or current is increasing, the output power is also increasing. Also, if either voltage or current decreases, the output power decreases. In addition, based on equation 3.24, the increment of duty cycle in Boost converter will change the output voltage to the same direction, meaning that increasing duty cycle will increase output voltage and vice versa. Therefore, using only load voltage measurement and direction of duty cycle increment, the nature of Perturb and Observe algorithm could be implemented.

The algorithm begins with sensing the load voltage and have it compared with the previous value. The current duty cycle is also compared with the previous one. If the voltage difference has the same direction or sign as duty cycle difference, then increase the recent duty cycle by a perturbation step of ΔD. On the other hand, if the voltage's difference

has reverse direction or sign as the duty cycle's difference, then decrease the recent duty cycle by ΔD. Figure 3.22 and 3.23 represent the flow chart and the block diagram of the single sensor load voltage MPPT algorithm, respectively.

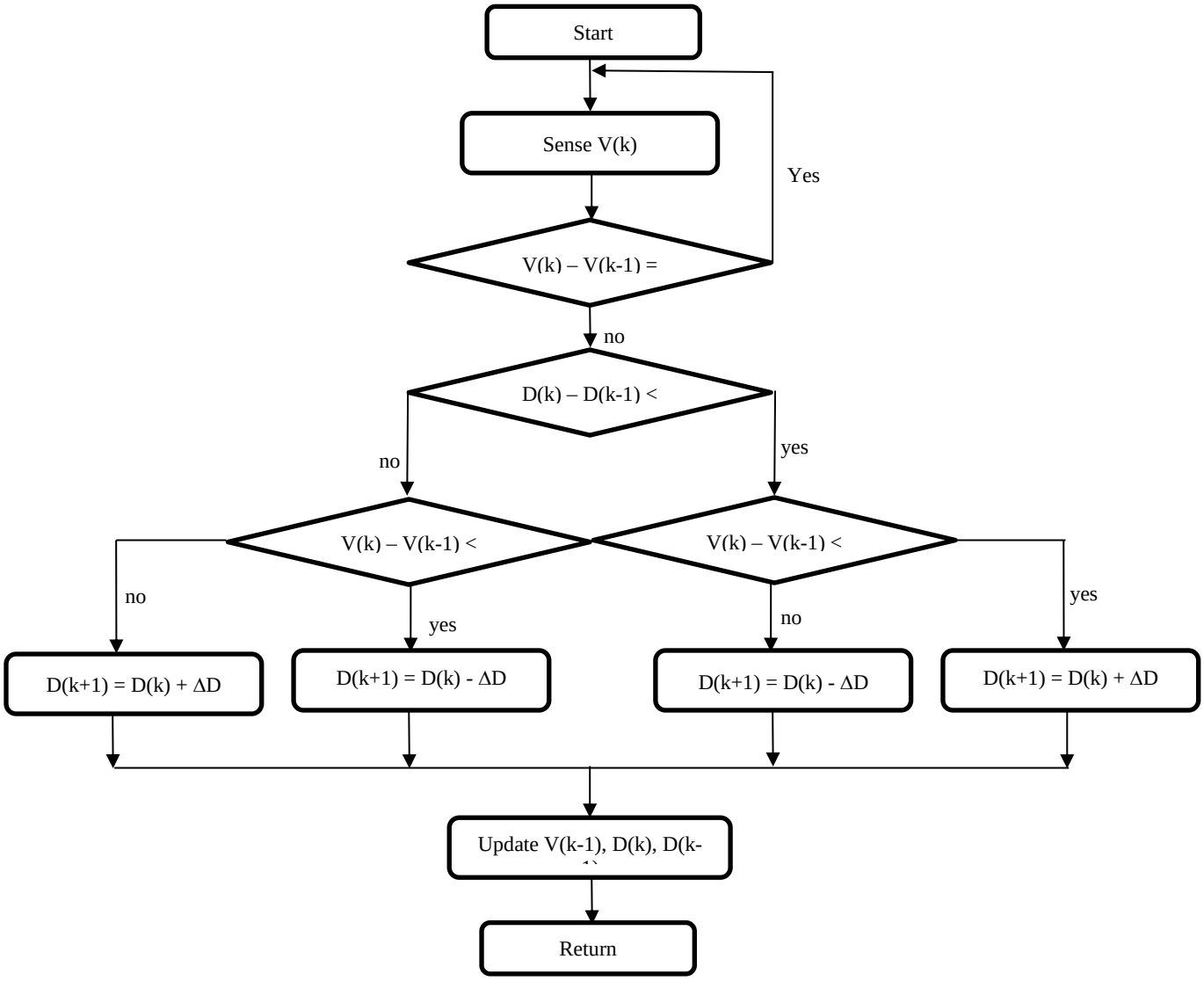

Figure 3.22. Single Sensor Load Voltage MPPT Algorithm

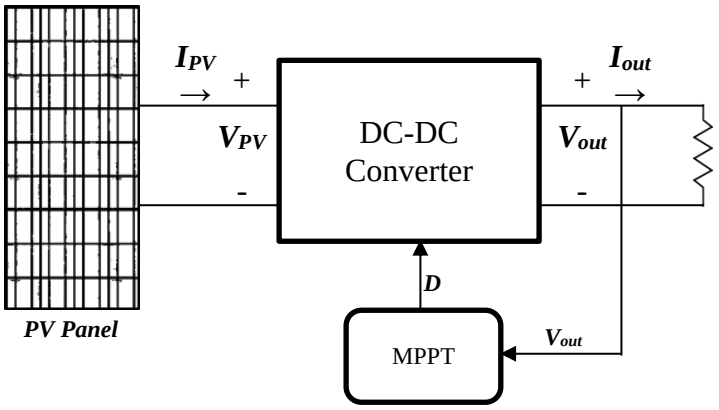

Figure 3.23. Single Sensor Load Voltage MPPT Configuration

Based on the discussion in Section 3.3.1 and 3.3.2, Single Sensor Load Voltage MPPT algorithm is chosen to be implemented in this experiment for several reasons. First, the algorithm only uses one voltage sensor at the output side of Boost converter, which implies the relatively lower complexity and cost of the controller circuit. In addition, fewer components mean that it is easier to control and maintain. Second, the simpler is the circuit and algorithm, the faster is the time response. Thus, the circuit will reach MPP faster.

3.4 SIMULATION RESULTS ON MATLAB/SIMULINK

Matlab/Simulink is used to verify the performance of the combined boost converter and single sensor load voltage MPPT algorithm. The simulation setup and the result are shown in Figure 3.24 and 3.25, respectively. PV array used in the simulation is a built in Matlab/Simulink model as discussed in Section 2.6. Further, the model of the PV Array follows Figure 2.9. There are two input signals of the simulation: solar irradiance and temperature. First, based on discussion in Section 2.5, the expected maximum irradiance generated in this experiment is 482.2 W/m^2. Thus, the input irradiance parameter used in

the simulation is 482.2 W/m^2. Second, the standard test temperature for pv panel that is used in this experiment is 25^oC, thus, the value is used as the simulation temperature parameter.

The MPPT algorithm as shown in Figure 3.22 is implemented in the gate control block. This simulation uses built in PWM Generator block to generate PWM signal based on MPPT algorithm. Then, the PWM signal controls the gate of the MOSFET directly.

To simulate a sudden change of irradiance and verify the circuit performance including the MPPT algorithm, in this simulation the solar irradiance instantaneously changes from 0 W/m^2 to 488 W/m^2.

Figure 3.25 shows that using the algorithm, the system effectively reaches MPP. Also as expected, the voltage level oscillates around MPP in corresponding to the duty cycle that change by the magnitude of ΔD.

Moreover, Figure 3.25 verifies that the relation between V and I at the output side of converter is linear. This confirms that a single sensor at the output side is enough to find out the direction of power change.

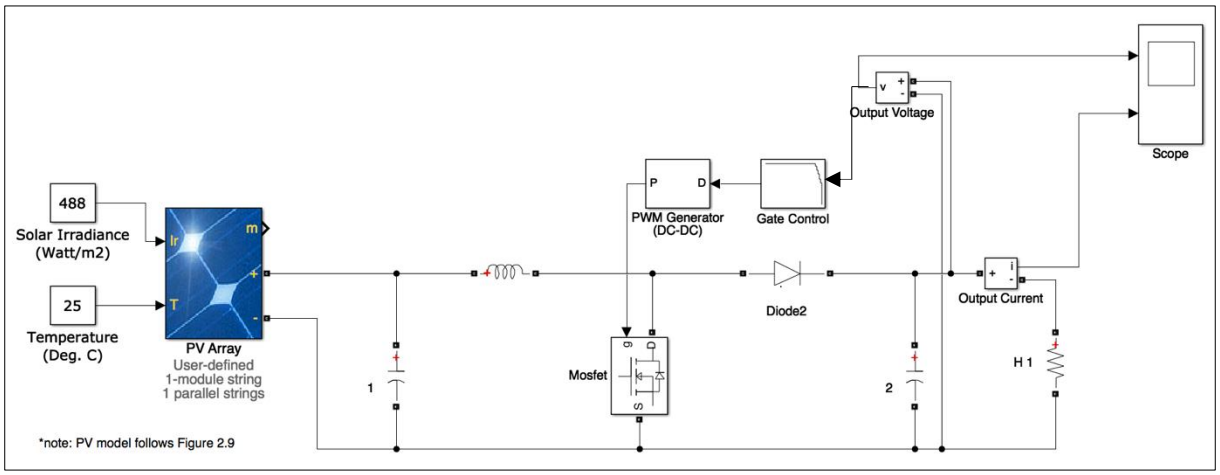

Figure 3.24. Simulation of Solar Simulation on MATLAB Matlab/Simulink

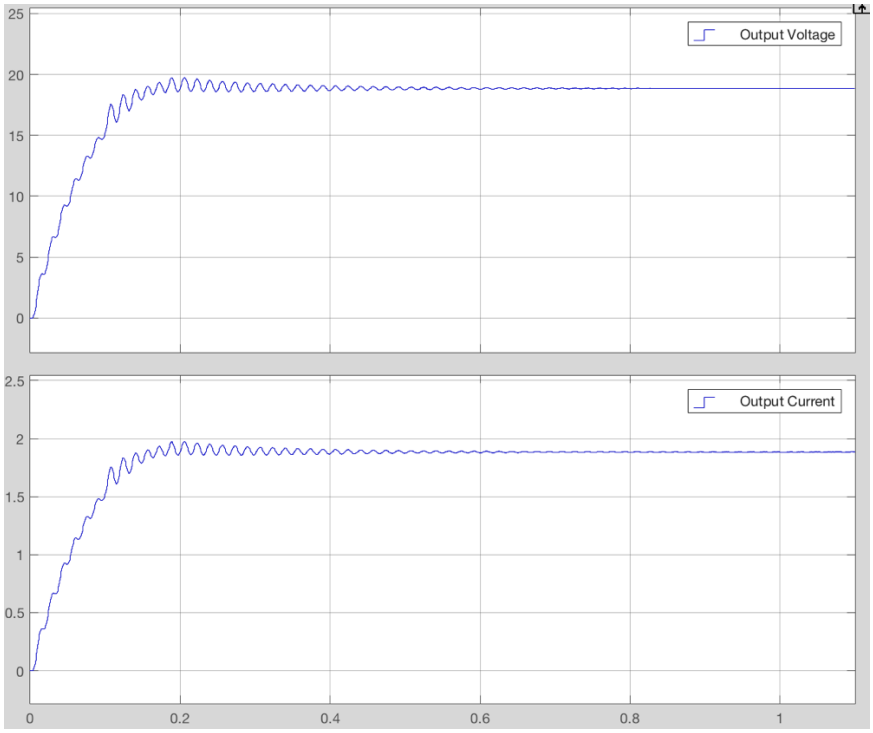

Figure 3.25. Transient of Boost Converter Output Voltage and Current in tracking MPP

3.5 CONFIGURATION AND COMPONENTS

The configuration will be divided into two sections: power and control. The power section is the DC-DC converter, and as described in Section 3.2, Boost Converter is selected. As for the control section, Tiva Launchpad TI4MC123 is selected as the main controller for three reasons. First, the microcontroller has an embedded Analog to Digital (ADC) functionality, which will be used to sense the load voltage. Second, it has PWM output pins, which are required to control duty cycle of the switch in the DC-DC converter. Finally, TI4MC123 uses C code which could easily implement the algorithm of Single Sensor Load Voltage MPPT.

3.5.1 Boost Converter's Components

The overall schematic of Boost Converter is shown on Figure 3.26.

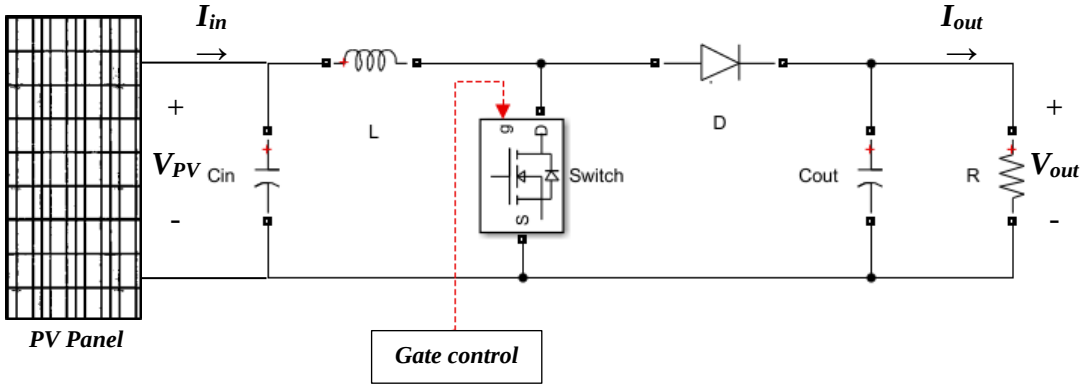

Figure 3.26. Detail Configuration of Boost Converter

The following calculations are used to select the value of inductor and output capacitor.

$$\Delta V = \frac{\Delta Q}{C} \tag{3.43}$$

$$\Delta Q = I_{out}T \tag{3.44}$$

The worst case of ripple happens when C_{out} discharge to the load at the longest period of time, in other words, when duty cycle D=1.

$$\Delta V = \frac{I_{out}T}{C} \tag{3.45}$$

$$T = \frac{1}{f} \tag{3.46}$$

$$\Delta V = \frac{I_{out}}{Cf} \tag{3.47}$$

Assuming that the maximum output current is 5.29 A, and maximum allowable output ripple voltage is 5% at switching frequency of 100 kHz, then the minimum capacitor required is 1058 μF.

Figure 3.27 is the boundary condition between continuous and discontinuous modes of the inductor.

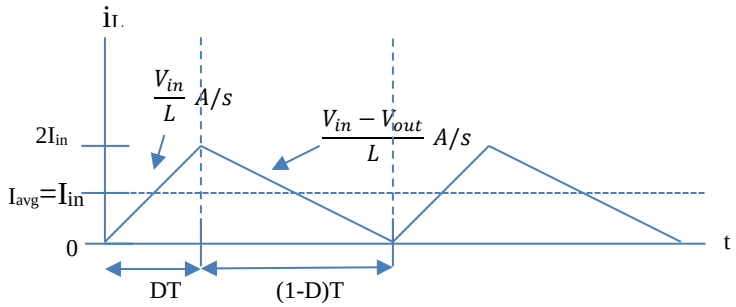

Figure 3.27. Inductor Average Current on Boundary Conduction Mode

For (1-D)T period of time;

$$-2I_{in} = \frac{V_{in}-V_{out}}{L_{boundary}}(1-D)T \tag{3.48}$$

$$L_{boundary} = \frac{V_{in}D}{2I_{in}f} \tag{3.49}$$

To guarantee the circuit always in continuous conduction mode, the inductor value must follow equation 3.49. The largest $L_{boundary}$ at a particular switching frequency occurs when D = 1. Thus, with a V_{in} max of 22.5 V, an I_{in} minimum of 0.7 A, and a switching frequency of 100 kHz, then minimum inductor L required is 0.16 mH.

$$L > \frac{V_{in}}{2I_{inf}} \tag{3.50}$$

3.5.2 Voltage Sensing Configuration

The actual load voltage on the DC-DC converter that is used in this experiment can reach up to 40 Vdc. However, the maximum input of analog to digital converter (ADC) on TI4MC123 is 3.3 Vdc, and thus, this actual voltage must be reduced before it is sent to microcontroller's pin. In addition, switching noise and other noise from the power section must be minimized in order to ensure accurate sensing. Figure 3.28 is the configuration of voltage sensing circuit.

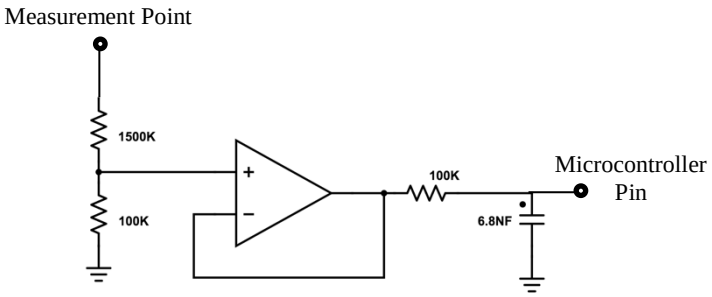

Figure 3.28. Voltage Sensing Circuit Configuration

First, using resistor in series, the actual voltage is reduced by ratio of

$$\frac{100}{100 + 1500}$$

thus the maximum voltage in microcontroller pin is:

$$V_{max(ADC)} = 40\left(\frac{100}{100 + 1500}\right) = 2.75\, Vdc$$

Next, the voltage divider is connected to a buffer circuit using OpAmp to ensure high impedance isolation. Finally, to prevent high frequency ripple noises getting into the microcontroller, a low pass filter using a shunt capacitor is used and placed before pin connection.

3.5.3 MOSFET Gate Firing Circuit

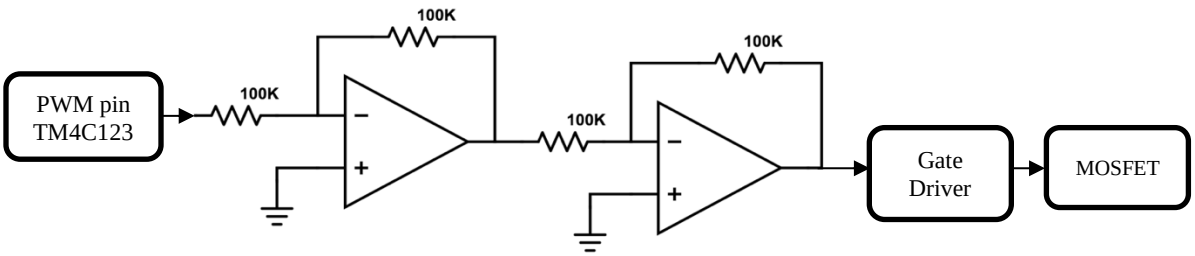

Figure 3.29. MOSFET Gate Firing Circuit Configuration

A firing circuit, as shown in Figure 3.29, is used to engage the gate of the MOSFET. The output voltage of the PWM pin on microcontroller TM4C123 is limited to 3.3 V. However, the operating range of the MOSFET gate is 4-18 V. Therefore, the circuit uses a gate driver that amplifies the PWM signal from the microcontroller. A Buffer circuit and cascaded unity inverting OpAmps, which provide high impedance isolation, are used between microcontroller TM4C123 pin and gate driver.

3.5.4 Single Sensor Load Voltage MPPT Algorithm Code

Translating the algorithm as shown in Figure 3.22, below is the Single Sensor Load Voltage MPPT code in C language, which is implemented in Microcontroller TM4C123:

```
while (1) { // infinite loops
dV = V-Vold; // comparison V(k) and V(k-1)
DeltaDC = f-g;          // f is D(k), g is D(k-1)
        if (DeltaDC!=0){       // DeltaDC is comparison D(k) and D(k-1)
          if (DeltaDC < 0)
                {if (dV < 0)
                                {DC = f + deltaD;} // deltaD is Duty cycle perturbation step
                        else
                                {DC = f - deltaD;}}
         else
                 {if (dV < 0)
                                {DC = f - deltaD;}
                        else
                                {DC = f + deltaD;}}}
        else
                {DC = f;}
if (DC >0.8) {DC = 0.8;}       // Max Duty Cycle
if (DC <0.05) {DC = 0.05;}    // Min Duty Cycle
g=f;     // Update D(k-1)
f=DC;  // Update D(k)
Vold = V;}      // Update V(k-1)
```

Chapter 4: Solar Simulator Validation

4.1 INTRODUCTION

This chapter will help further verify and validate the complete circuit of solar simulator that has been built. Figure 4.1 shows the diagrams of the complete simulator. Each component of the simulator works sequentially. Therefore, it is easier first to validate them component by component then validate the complete system. For this purpose, the complete simulator is broken down into 5 main components and the input and output of each component will be observed: Artificial light, Control Ballast, PV Panel, Boost Converter, and MPPT Algorithm.

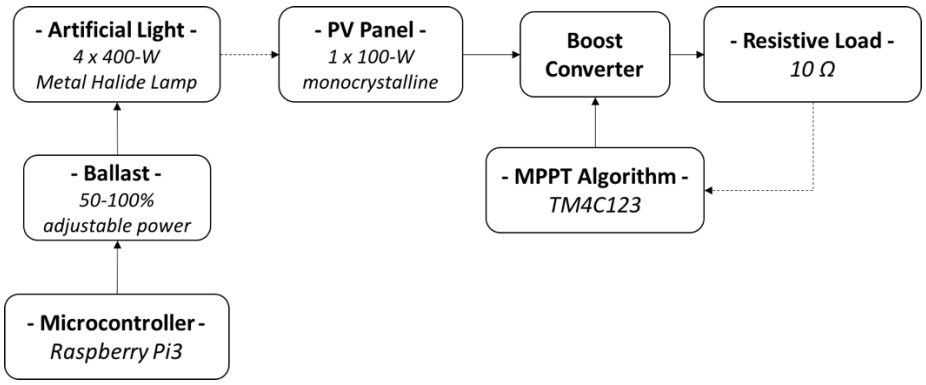

Figure 4.1. Complete Solar Simulator Configuration

4.2 ARTIFICIAL LIGHT

Power and light illumination are the two items to be validated for this component. First, the artificial light used in this experiment is a four metal halide arc lamp with a 400-watt power rating. The power absorbed by 4 bulbs is measured, and the results are as follows,

V_{in} : 224.7 V

I_{in} : 7.98 A

P_{in} : 1772 VA

Assuming a power factor of 0.9, the power absorbed by the bulbs is 1595 Watts which matches the total bulbs power rating. Second, Illumination of the four bulbs is measured on the surface of the panel. There are five measurement points as shown in Figure 4.2. The results are as the following,

1. 174,385 lux
2. 129,566 lux
3. 133,616 lux
4. 121,656 lux
5. 113,301 lux

The average illumination is 134,504.8 lux. The result is higher than expected. However, using the same lux meter, direct sun illumination on a bright day is also measured and the result is 187,967 lux which is higher than normal value of 100,000 lux. It is observed that the light meter has a different calibration standard. Nevertheless, as discussed and expected on Section 2.5, the artificial light in this experiment produce less illumination than the illumination of 1-sun.

The artificial light used in this experiment has a class B spectral content which deviates ± 40% from sun's spectral contents [2]. Based on [19], illumination is linear with sun irradiance. And further, by taking light spectral content into account, the expected

output power from PV panel is about $P = \frac{134504}{187967}(1 \pm 40\%) = 42\% - 100\%$ of its rating.

The rating of PV panel is 100 W, thus, the expected output power is 42-100 Watt.

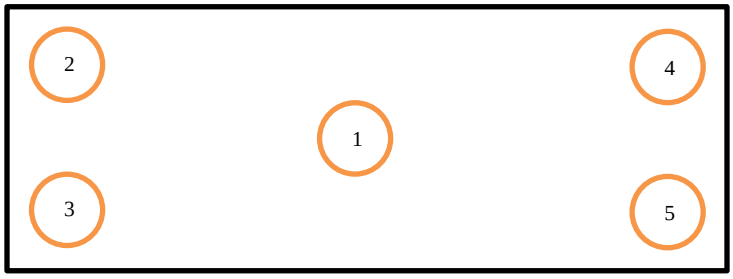

Figure 4.2. Illumination Measurement Points

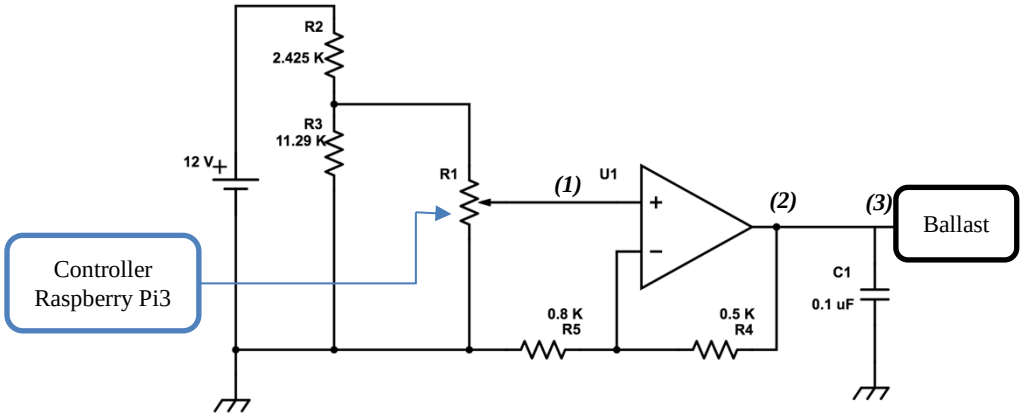

Figure 4.3. Voltage Validation Points on Ballast Control Circuit

4.3 BALLAST AND CONTROL

4.3.1 Control

Ballasts validation begins with verifying control voltage produced by the control circuit. Figure 4.3 is the control circuit of the ballast. Table 4.1 shows the measured voltage at the wiper of Digital Potentiometer, Non-inverting OpAmp, and Ballast control terminal

correspond to digital input from microcontroller. The measuring points are noted by (1), (2), and (3) in Figure 4.3.

Digital Potentiometer Input	Digital potentiometer Wiper Voltage (1)	Non Inverting OpAmp output Voltage (2)	Ballast control terminal Voltage (3)
0	5.65	9.17	9.17
31	4.77	7.75	7.75
63	3.45	5.62	5.61
95	1.88	3.07	3.07
127	0.08	0.15	0.15

Table 4.1. Voltage Measurement on Ballast Control Circuit

Based on Table 4.1, the voltages on control terminal of the ballast are within operating range, which is 0-10 V. Further, by plotting the digital-potentiometer input from microcontroller and the ballast control voltage into a x-y plane as shown in Figure 4.4, it is observed that both of them are linear with an error of $R^2 = 0.9854$.

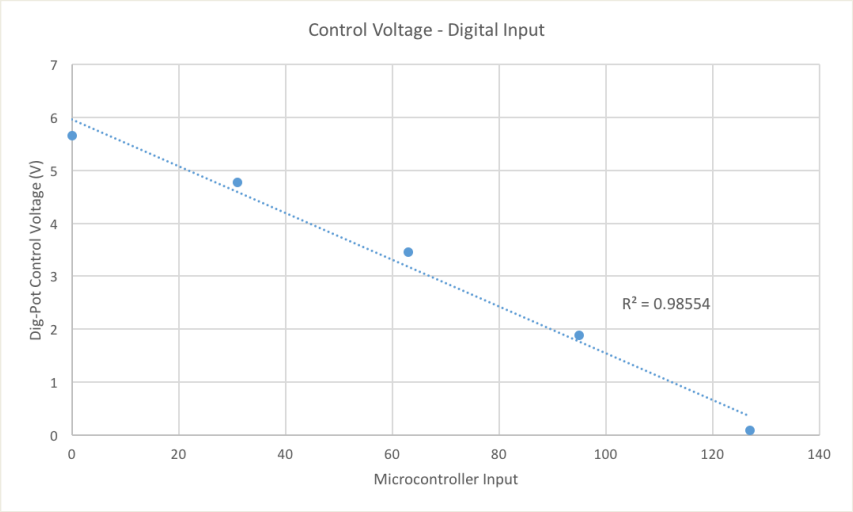

Figure 4.4. Curve of Digital Input – Digital Potentiometer Voltage

4.3.2 Power

Table 4.2 shows the measurement of power absorbed by light bulbs on three different digital input from microcontroller. The absorbed power at the largest digital input (127) or at the lowest irradiance is about 52.4% compared to its smallest digital input (0) or highest irradiance. Based on discussion in Section 2.5, the light bulb absorbs 50% of its rating power when produces minimum irradiance, and absorbs 100% of its rating power when produces maximum irradiance. Thus, it is confirmed that the ballast works as expected.

Input Microcontroller	Ballast Control Voltage	Ballast Input Current	Absorbed Power
127	0.15	4.14 A	930 W
0	9.17	7.9 A	1772 W

Table 4.2. Power Measurement on Ballast

4.3.3 Transient Time

As discussed in Section 4.3.1 and 4.3.2, a particular digital input value from microcontroller will correspondence with a particular ballast control voltage and absorbed power. And thus, changing the digital input value will change the absorbed power. The microcontroller and control circuit is capable to change the value instantaneously, however, the ballast and an arc lamp require longer time to change into a new state.

The transient time from ballast receiving control voltage until it completely changes into a corresponding state is measured and shown in Table 4.3. Darkest-brightest and brightest-darkest are the only two conditions that are measured because these are the biggest change of microcontroller input.

Ballast's transient time is important since it determines the required minimum intermediate time before a new irradiance data can be updated into the simulator.

Condition	Digital Input Microcontroller	Ballast transient time
Darkest to Brightest	127 to 0	29 s
Brightest to Darkest	0 to 127	60 s

Table 4.3. Measurement Result of Ballast Transient Time

The maximum transient time is 60 seconds, which implies that the minimum time of updating the irradiance data in this solar simulator system is 60 seconds. Otherwise, before completing a particular state, the simulator already starts to change into another state.

4.4 PHOTOVOLTAIC (PV) PANEL

The validation of the PV panel is done by measuring the output voltage, current, and power of the panel under artificial light condition.

Based on discussion in section 2.5, The maximum expected output power of pv panel is 48.2 Watt. The actual measurement using 11 Ω loads is as follows,

V_{Load} : 22 V

I_{Load} : 2.159 A

P_{Load} : 47.49 W

The output power is 1.5% lower than expectation, however, it is acceptable and in agreement with discussion in Section 4.2.

4.5 DC-DC CONVERTER

There are several items that must be verified for Boost Converters. The first one is V_{in}/V_{out}, switch or MOSFET performance, and finally ripple on V_{out}.

4.5.1 V_{in}/V_{out}

Validating V_{in}/V_{out} relation starts first by measuring V_{in} and V_{out} at several values of duty cycle and then comparing the measurements with the expected value using equation 3.24. The measurement results using 11Ω loads are shown in table 4.4. The result shows that there is a discrepancy between expected and measured V_{out}. This discrepancy is expected due to the losses from 100 kHz switching is considerably large. Another possible reason is miss reading of the duty cycle value. However, actual V_{in}/V_{out} relation follows the curve of equation 3.24 and the discrepancy is relatively consistent for all duty cycle value measurements, thus verifying that the boost converter works.

V_{in} (V)	Duty Cycle	Expected V_{out} (V)	Measured V_{out} (V)
12.1	0	12.09	10.35
12.1	0.1	13.43	11.64
12.1	0.2	15.11	13.5
12.1	0.4	20.15	17.8
12.1	0.6	30.22	25

Table 4.4. Measurement of V_{in} and V_{out} of Boost Converter

4.5.2 MOSFET

The validation of MOSFET starts by verifying PWM signal from the microcontroller and gate driver. Figure 4.5 and 4.6 represent the measurement of PWM

signal at the output pin of Microcontroller and Gate driver respectively. It shows that the output of the gate driver is in accordance with microcontroller output and is within the operating range voltage of the MOSFET's gate, which is 4-16 V [20].

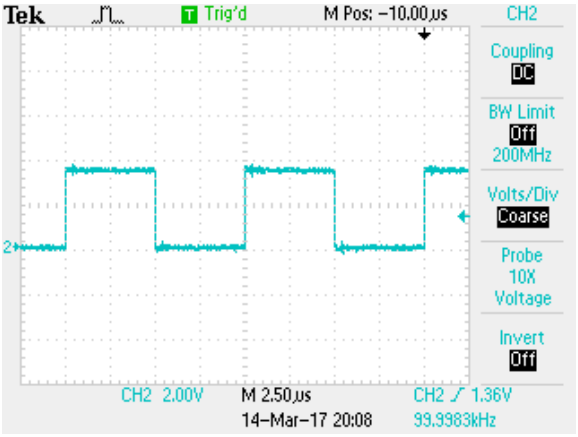

Figure 4.5. PWM Signal on TM4C123 Output Pin

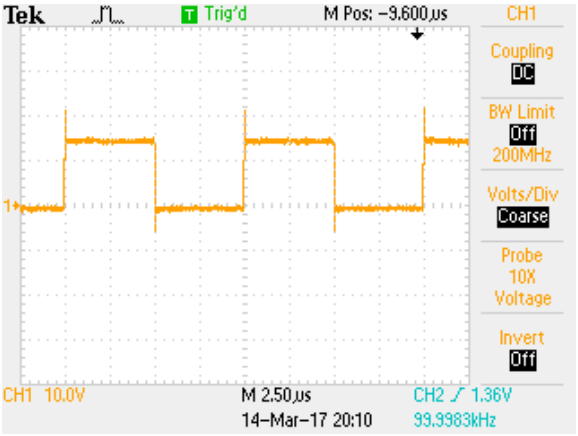

Figure 4.6. PWM Signal on Gate Driver Output

Figure 4.8, 4.9, and 4.10 show V_{GS}, V_{DS}, and V_{DS} with snubber of the MOSFET, respectively. Because of the internal capacitance and inductance of the MOSFETgate, the shape of V_{GS} is much more distorted compared to the output of microcontroller. However, the shape in this case will not cause an issue since the voltage level given to the gate is 12

V which is higher than the gate threshold voltage of 4 V, therefore, the on/off performance of the switch is not affected.

Further, due to drain-source internal capacitance, the ringing voltage is relatively large, and the ringing frequency is very high as shown in Figure 4.9. Thus, it requires snubber capacitor and resistor as shown on Figure 4.7. The resistance and capacitance value of the snubbers follows the manufacturer's recommendation practice and MOSFET datasheet [21]. Figure 4.9 shows the ringing voltage during switch on/off of the MOSFET after placing snubber capacitor and resistor across the drain and source.

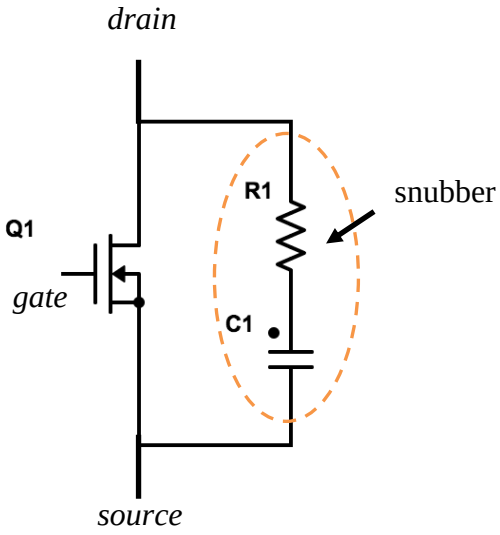

Figure 4.7. Snubber Circuit as per manufacturer's recommendation practice

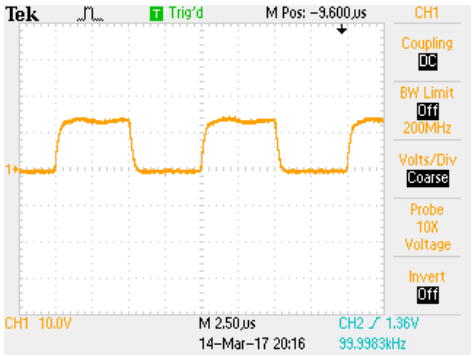

Figure 4.8. PWM signal on MOSFET Gate

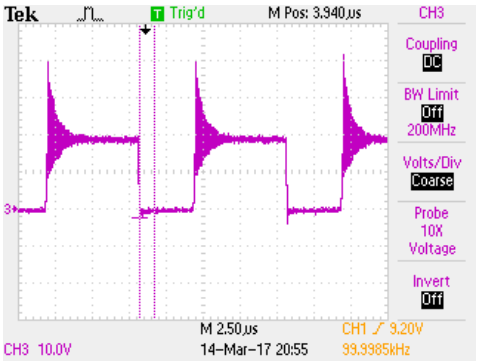

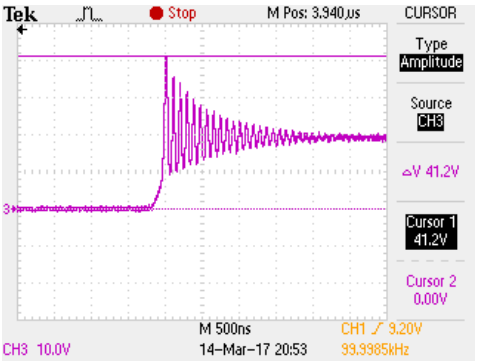

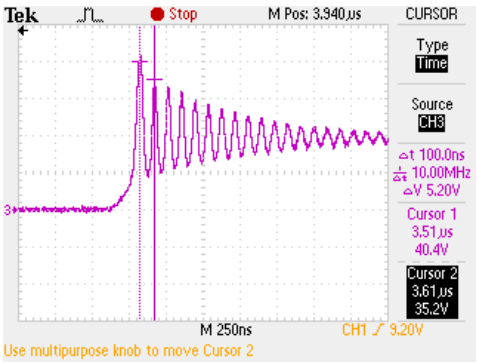

Figure 4.9. V_{DS} of MOSFET

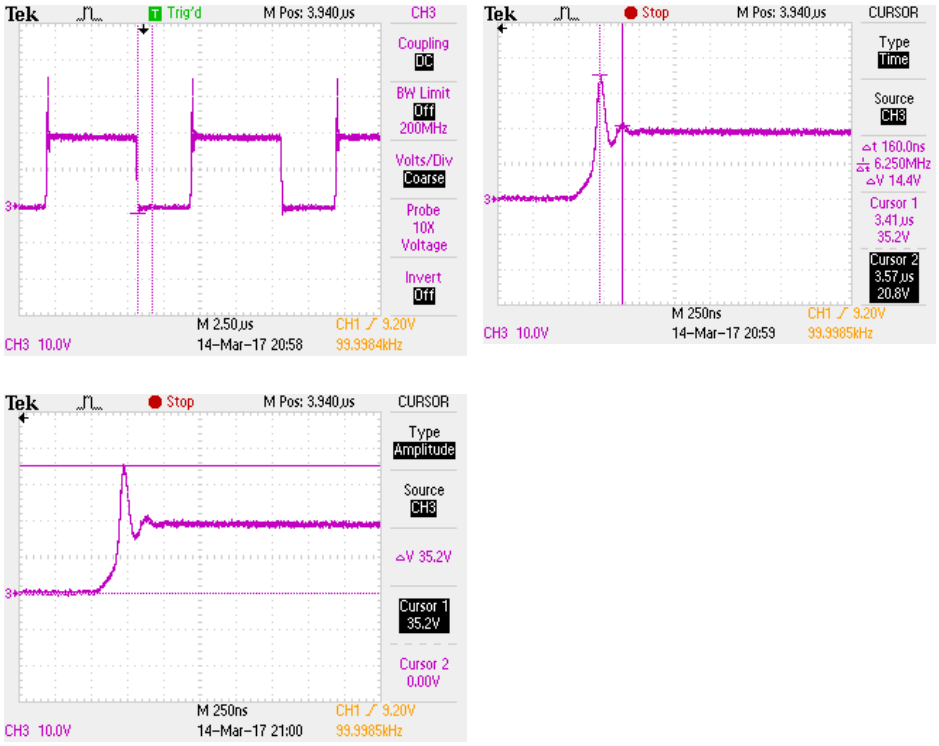

Figure 4.10. V_{DS} of MOSFET with snubber Resistor and Capacitor

Based on the discussion in Section 3.2, for safety reasons, the duty cycle of the gate is limited to 0.8. Figure 4.11 and 4.12 represent V_{ds} during duty cycle is 0 and 0.8, respectively. It shows that DC-DC converter always works on the continuous mode across the duty cycle operation range.

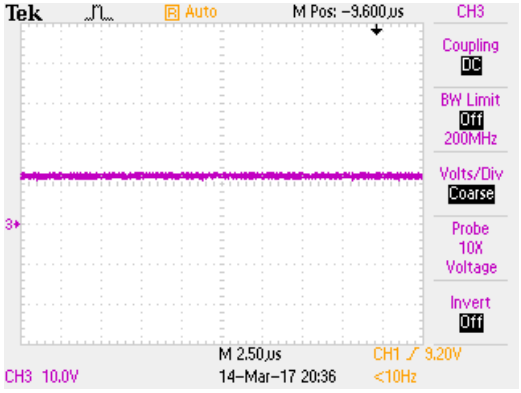

Figure 4.11. V_{DS} during Duty Cycle is 0

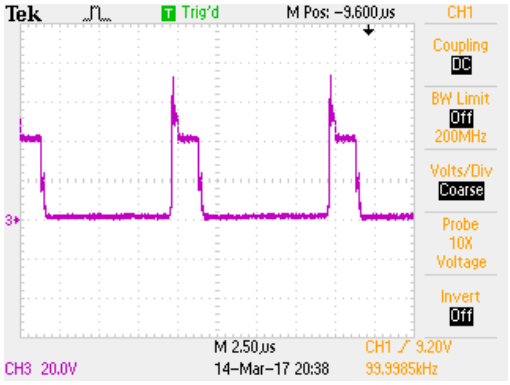

Figure 4.12. V_{DS} during Duty Cycle is 0.8

4.5.3 Output Ripple Voltage

Figure 4.13 shows the output ripple voltage measurement. The maximum ripple is 75 mV or 0.625% which is below the expected value of 5%.

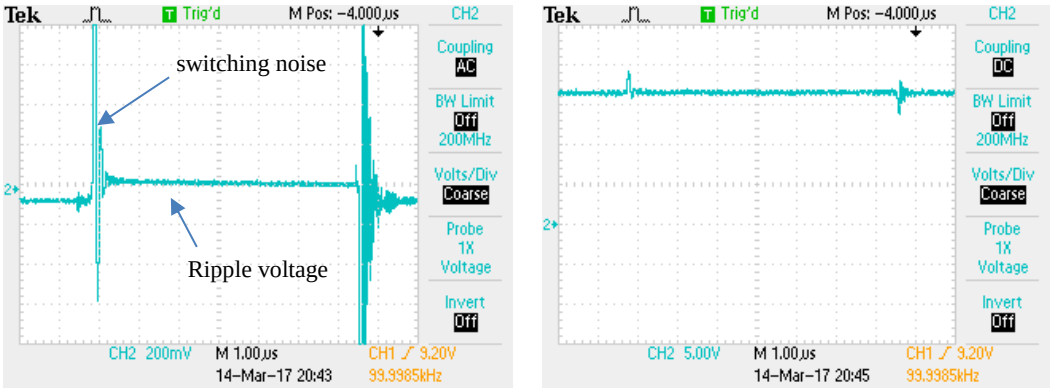

Figure 4.13. Output Ripple Voltage

4.6 MPPT ALGORITHM

Validating the MPPT algorithm requires all of the simulator components to be integrated. It is basically verifying the performance of the complete simulator system. The validation starts by setting the digital input of the potentiometer into 3 different states: 100, 69, and 0. Those values represent cloudy, partly cloudy, and sunny conditions, respectively. Next, the output power of the simulator without MPPT, with manual MPPT, and with MPPT algorithm is observed and compared. Table 4.5 shows the comparison value.

Manual MPPT does not employ any algorithm, therefore a temporary control circuit which apply a potentiometer to vary the duty cycle of the MOSFET is used. The duty cycle of the MOSFET gate is adjusted by rotating the potentiometer until reach MPP.

In the case of without MPPT, the pv panel is connected directly to the load.

Input Microcontroller	Irradiance level (W/m^2)	No MPPT (Watt)	Manual MPPT (Watt)	MPPT algorithm (Watt)	Deviation Manual MPPT and MPPT Algorithm
100	308	16.912	18.123	17.598	2.8 %
69	665	19.725	28.907	29.376	1.6 %
0	1400	20.695	47.916	47.298	1.2 %

Table 4.5. Comparison of Output Power with and without MPPT

Based on Table 4.13, as expected, the output power of pv panel using MPPT is higher than without MPPT. Further, the result of manual MPPT and MPPT algorithm matches with an average deviation of 1.8%. Thus, it is verified that the MPPT algorithm effectively reach MPP.

Figure 4.14, 4.15, and 4.16 show the measurements of simulator transient time using digital oscilloscope. The time resolution for those figures are 10 s/Div, 10 s/Div, and 25 s/Div, respectively. Figure 4.14 shows the transient time of the simulator from lowest to highest irradiance level, which is about 30 seconds. Figure 4.15 shows the transient time from highest to the lowest irradiance level, which is 60 seconds. Figure 4.16 shows a transient time for the lowest-highest-lowest irradiance level scenario.

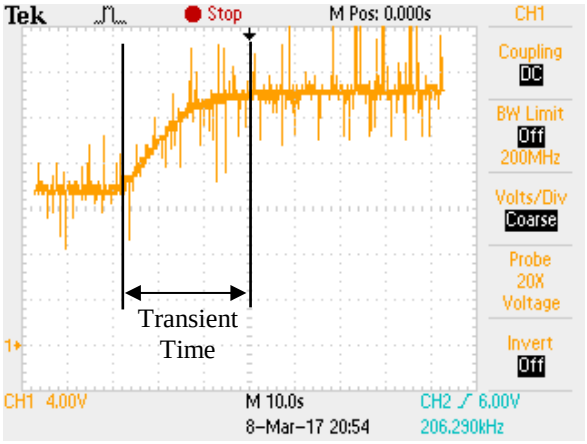

Figure 4.14. Output Voltage Transient during Irradiance Change from Lowest to highest

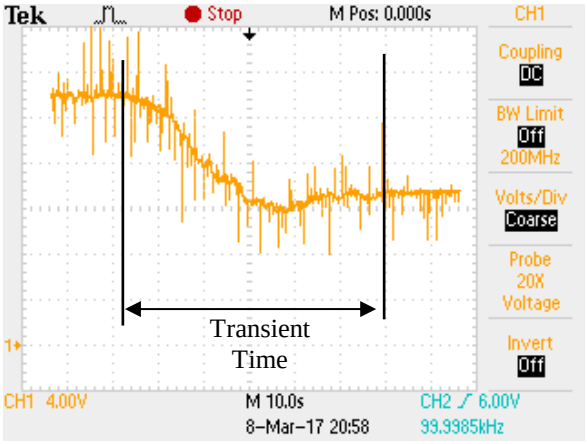

Figure 4.15. Output Voltage Transient during Irradiance Change from Highest to Lowest

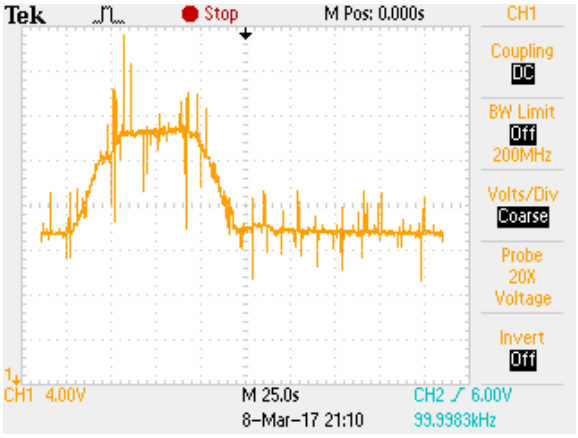

Figure 4.16. Output Voltage Transient during Irradiance Change from Lowest-Highest-Lowest

The transient time of the ballast and the complete simulator system is the same. Thus, this verifies that the ballast is the limiting factor of the system transient time.

4.7 EXPERIMENTAL RESULTS

Based on discussion in Section 2.7, June 1st, July 1st, and August 1st on 2015 are selected as the solar irradiance profile to be simulated in this experiment. However, simulating all the data with 60 seconds of transient time, will take three full days to complete. Therefore, to optimize and shorten the experiment time, 55 data points on the most fluctuating periods and covering the largest irradiance change during those three days are selected. Figure 4.17 shows the selected 55 solar irradiances to be simulated.

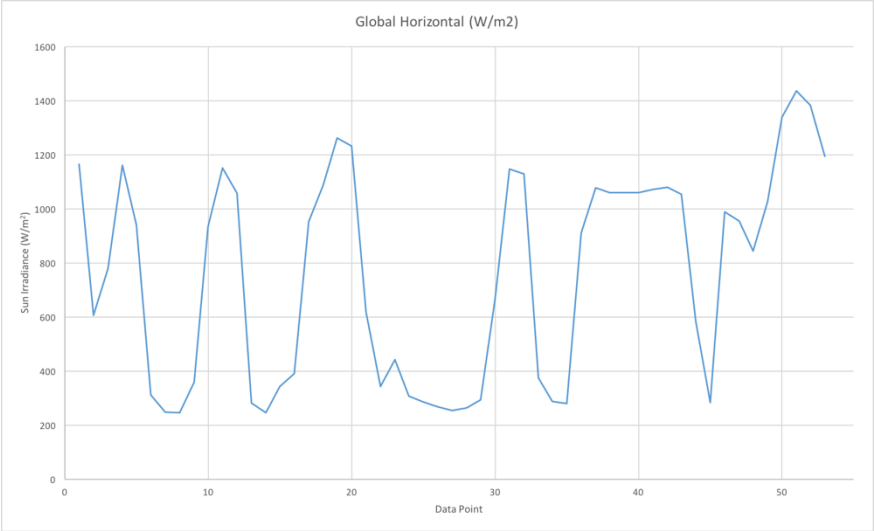

Figure 4.17. Selected Actual Irradiance Profile

The actual solar irradiance data has a 1-minute resolution. In other words, each data point is sampled every 1 minute in actual condition. The maximum transient time of the ballast in responding to the input control is 1 minute. Thus, in this case, the simulator is set

to update the irradiance data into the ballast every 1 minute. Figure 4.18 represents the output of the simulator corresponding to solar irradiance fluctuation. It shows that the output power of the simulator follows the irradiance profile linearly.

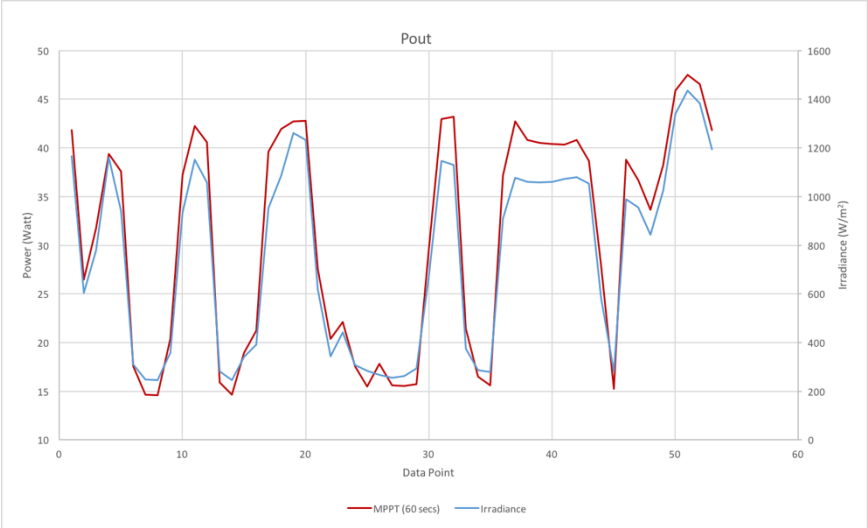

Figure 4.18. Output Power of Solar Simulator with 60 s update

As mentioned in Section 2.5, due to ballast's limited ability on delivering power to the light bulbs, the minimum irradiance that could be simulated is 10% of the maximum irradiance on the actual solar irradiance profile. In addition, 60 seconds is the transient time from the brightest (100% irradiance) to the darkest (10% irradiance) condition. In this experiment, the change of irradiance (delta irradiance) from 100% to 10% is equal to 1260 W/m^2. In other words, 60 seconds of transient time occurs when delta irradiance is 1260 W/m^2. Thus, if the delta irradiance is lower than 1260 W/m^2, the transient time of the system will be shorter than 60 seconds.

At all times, simulation data that is used in this validation has a delta irradiance lower than 1260 W/m^2, thus, a shorter transient time is expected. To confirm this, an

experiment which updates the solar irradiance data every 30 seconds is completed and the result is shown in Figure 4.19. It shows that during negative delta irradiance (decrease of irradiance) at a few points, the output power is slightly higher compared to the 60 seconds simulation. This means that the simulator is still in a transient state when receiving a new irradiance update. Overall, however, the result is relatively similar between the 30 seconds and the 60 seconds simulations.

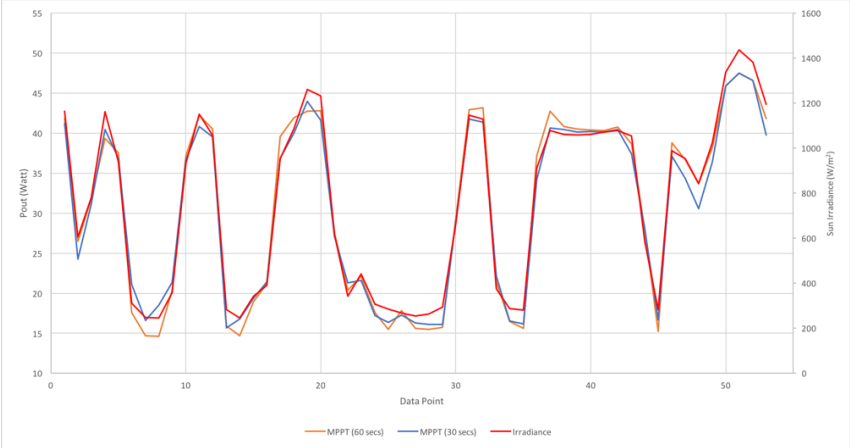

Figure 4.19. Output Power of Solar Simulator with 60s and 30s update

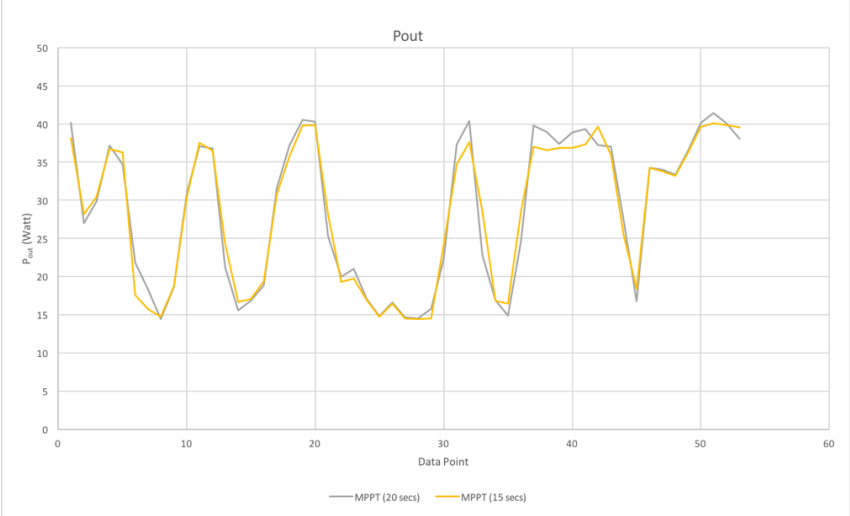

Figure 4.20. Output Power of Solar Simulator with 20s and 15s update

Upon further investigation of the simulator's transient time, experiment with 20 seconds and 15 seconds update time are completed, and the results are shown in Figure 4.20. Figure 4.21 shows a comparison of 15, 20, 30, and 60 seconds simulation time. At all times, output power on 20 secs and 15 seconds results, shows a lower value during positive delta irradiance (increase of irradiance) and higher value during negative delta irradiance (decrease of irradiance). This implies that 20 seconds and 15 seconds are not enough time for simulator to finish its transient period and reach a new MPP state, in this particular, a new solar irradiance value.

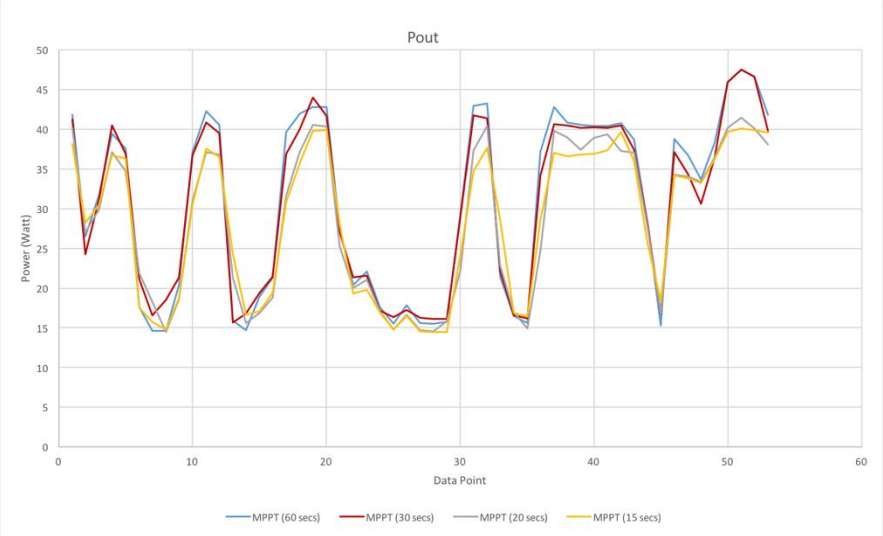

Figure 4.21. Comparison Output Power of Solar Simulator with 60s, 30s, 20s, and 15s update

To summarize, this simulator is capable of simulating any irradiance profile with 60 seconds of transient time. However, depending on the maximum delta irradiance during the particular irradiance profile, transient time can be improved.

Chapter 5: Conclusion and Future Works

5.1 CONCLUSION

The final goal of this work is to build a low cost and effective solar simulator integrated with PV system and capable of reproducing actual solar irradiance profile. For that purpose, in this thesis, several types and classifications of solar simulator based on IEC and ASTM standard are presented. Moreover, three types of DC-DC converters are presented in order to show their functionality and effectiveness in reaching Maximum Power Point of the PV system. The popular Perturb and Observe MPPT technique is also presented and compared to the proposed technique of Single Sensor Load Voltage MPPT algorithm. Based on those descriptions and comparisons, Continuous type Solar Simulator, a DC-DC Boost converter, and Single Sensor Load Voltage MPPT algorithm are chosen and are used to construct the complete integrated solar simulator. As for embedded systems, Raspberry Pi3 and Launch Pad TI4MC123 which are available in the commercial market, are used to link the algorithm and the analog circuits. The simulation of the complete simulator using Matlab/Simulink to verify the complete system is also presented. The simulation shows that the system effectively simulates actual solar irradiance profile and reaches MPP.

After the simulation, the actual solar simulator is built. Each component is validated, and the input and output of each component are observed to ensure that the values are correct and expected. Finally, the simulator is tested using actual solar irradiance profile from University of Texas Pan-American Edinburg, Texas in 2015. The simulator

effectively reproduces the actual solar irradiations profile, and PV systems along with MPPT algorithm successfully produce maximum possible output power which corresponds to the instantaneous irradiance.

5.2 FUTURE WORK

There are several possible future projects related to this work. The first would investigate ways to improve simulator's transient time. Transient time of the built solar simulator is 60 seconds which implies that the finest resolution of actual solar irradiance profile that can be simulated is 60 seconds. Any actual data that has resolution smaller than 60 seconds cannot be reproduced exactly as the actual condition. Thus, a simulator that has a faster transient time would be beneficial.

The second would be investigating the effectiveness of the system on several PV panels. An array of panels are required in the simulation scenario that demand more power, and thus the effectiveness of Single Sensor Load Voltage algorithm on arrays of PV must be investigated and revalidated.

Another related line of research would be building the inverter and then, integrating the simulator to the grid. Thus, the simulator could be used to observe the behavior of the grid after solar energy utilization in a controlled condition. Moreover, an inverter with reactive power control capability or a smart inverter could greatly extend the application of the simulator.

References

1. "Solar Industry Facts and Figures." *SEIA*. N.p., n.d. Web. 24 Mar. 2017. <http://www.seia.org/research-resources/solar-industry-data>.
2. Standard Specification for Solar Simulation for Photovoltaic Testing, ASTM standard E927-10, 2005.
3. Solar Simulator Performance Requirements, IEC Standard 60904-9, 2007
4. "Blog Archives." *TS-Space Systems - Solar Simulators and Vacuum Testing*. N.p., n.d. Web. 24 Mar. 2017. <http://www.ts-space.co.uk/news/archives/06-2015>.
5. Ribas, Javier, J. Marcos Alonso, Antonio J. Calleja, Emilio Lopez, Jesus Cardesin, Jorge Garcia, and Manuel Rico. "Arc Dynamic Stabilization in Low-Frequency Square-Wave Electronic Ballast for Metal Halide Lamps." *IEEE Transactions on Power Electronics* 22.5 (2007): 1592-599. Web.
6. *IESNA lighting handbook*. New York: Illuminating Engineering Society of North America, 2000. Print.
7. Vanek, Francis M., Louis D. Albright, and Largus T. Angenent. *Energy systems engineering: evaluation and implementation*. New York: McGraw-Hill, 2016. Print.
8. Yi, Li Feng, Kai Ru Zhang, and Jun Liu. "Fractional Order Modeling and Analysis of Buck-Boost Converter." *Applied Mechanics and Materials* 789-790 (2015): 842-48. Web.
9. Shebani, Muamer M., Tariq Iqbal, and John E. Quaicoe. "Comparing bisection numerical algorithm with fractional short circuit current and open circuit voltage methods for MPPT photovoltaic systems." *2016 IEEE Electrical Power and Energy Conference (EPEC)* (2016): n. pag. Web.
10. Sandali, Abdelhalim, Tarik Oukhoya, and Ahmed Cheriti. "Modeling and design of PV grid connected system using a modified fractional short-circuit

current MPPT." *2014 International Renewable and Sustainable Energy Conference (IRSEC)* (2014): n. pag. Web.

11. Bahari, Mohammad Iman, Pouya Tarassodi, Yousef Mazaheri Naeini, Ali Kalantari Khalilabad, and Paimaneh Shirazi. "Modeling and simulation of hill climbing MPPT algorithm for photovoltaic application." *2016 International Symposium on Power Electronics, Electrical Drives, Automation and Motion (SPEEDAM)* (2016): n. pag. Web.

12. Blange, Radak, Chitralekha Mahanta, and Anup Kumar Gogoi. "MPPT of solar photovoltaic cell using perturb & observe and fuzzy logic controller algorithm for buck-boost DC-DC converter." *2015 International Conference on Energy, Power and Environment: Towards Sustainable Growth (ICEPE)* (2015): n. pag. Web.

13. Rajani, Sachin Vrajlal, and Vivek J. Pandya. "Simulation and comparison of perturb and observe and incremental conductance MPPT algorithms for solar energy system connected to grid." *Sadhana* 40.1 (2015): 139-53. Web.

14. Ahmed, Emad M., Mohamed Orabi, and Masahito Shoyama. "High efficient variable step size incremental resistance maximum power point tracker for PV battery charging applications." *2013 IEEE Energy Conversion Congress and Exposition* (2013): n. pag. Web.

15. Boonmee, Chaiyant, and Yuttana Kumsuwan. "Implementation of ripple correlation control MPPT for single-phase VSI grid-connected PV systems." *2015 12th International Conference on Electrical Engineering/Electronics, Computer, Telecommunications and Information Technology (ECTI-CON)* (2015): n. pag. Web.

16. Qahouq, Jaber Abu, Yuncong Jiang, and Wangxin Huang. "Load-voltage-based single-sensor MPPT controller for multi-channel PV systems." *2014 IEEE Applied Power Electronics Conference and Exposition - APEC 2014* (2014): n. pag. Web.

17. Jiang, Yuncong, Jaber A. Abu Qahouq, and Tim A. Haskew. "Adaptive Step Size With Adaptive-Perturbation-Frequency Digital MPPT Controller for a Single-Sensor Photovoltaic Solar System." *IEEE Transactions on Power Electronics* 28.7 (2013): 3195-205. Web.

18. Killi, Muralidhar, and Susovon Samanta. "Output voltage sensor based maximum power point tracking for PV system using SEPIC." *2015 IEEE International Conference on Industrial Technology (ICIT)* (2015): n. pag. Web.

19. Treado, S., and T. Kusuda. *Solar Radiation and Illumination*. Washington: National Bureau of Standards, 1981. Print.

20. "FDA59N25 Fairchild Semiconductor | Mouser." *Mouser Electronics*. N.p., n.d. Web. 24 Mar. 2017.

21. "Resistor-Capacitor (RC) Snubber Design for Power Switches." *Resistor-Capacitor (RC) Snubber Design for Power Switches | DigiKey*. N.p., n.d. Web. 24 Mar. 2017.

22. "National Solar Radiation Data Base." National Solar Radiation Data Base. N.p., n.d. Web. 24 Mar. 2017. <http://rredc.nrel.gov/solar/old_data/nsrdb/>.

23. "Documentation." Implement PV array modules. - Simulink. N.p., n.d. Web. 12 Apr.2017.<https://www.mathworks.com/help/physmod/sps/powersys/ref/pvarray.html>.

24. Andreas, Afshin Michael. NREL: MIDC/University of Texas Panamerican Solar Radiation Lab (26.49 N, 98.17 W, 45 m, GMT-6). N.p., n.d. Web. 12 Apr. 2017. <https://www.nrel.gov/midc/utpa_srl/>.

25. Littlefair, P. J. "The luminous efficacy of daylight: a review." Lighting Research and Technology 17.4 (1985): 162-82. Web.

26. Index of /education/QLTkit/ACTIVITY_Documents/Safety. N.p., n.d. Web. 14 Apr.2017. <https://www.noao.edu/education/QLTkit/ACTIVITY_Documents/Safety / LightLevels_outdoor+indoor.pdf>.